energies

MDPI

Article

Active Vehicle Suspension with Anti-Roll System Based on Advanced Sliding Mode Controller

Jarosław Konieczny *, Marek Sibielak and Waldemar Rączka

Department of Process Control, AGH University of Science and Technology, Al. Mickiewicza 30, 30-059 Krakow, Poland; sibielak@agh.edu.pl (M.S.); waldemar.raczka@agh.edu.pl (W.R.)

* Correspondence: koniejar@agh.edu.pl

Received: 9 August 2020; Accepted: 21 October 2020; Published: 23 October 2020

Abstract: In the paper authors consider the active suspension of the wheeled vehicle. The proposed controller consists of a sliding mode controller used to roll reduction and linear regulators with quadratic performance index (LQRs) for struts control was shown. The energy consumption optimization was taken into account at the stage of strut controllers synthesis. The studied system is half of the active vehicle suspension using hydraulic actuators to increase the ride comfort and keeping safety. Instead of installing additional actuators in the form of active anti-roll bars, it has been decided to expand the active suspension control algorithm by adding extra functionality that accounts for the roll. The suggested algorithm synthesis method is based on the object decomposition into two subsystems whose controllers can be synthesized separately. Individual suspension struts are controlled by actuators that use the controllers whose parameters have been calculated with the LQR method. The mathematical model of the actuator applied in the work takes into account its nonlinear nature and the dynamics of the servovalve. The simulation tests of the built active suspension control system have been performed. In the proposed solution, the vertical displacements caused by uneven road surface are reduced by controllers related directly to suspension strut actuators.

Keywords: sliding mode controller; active vehicle suspension; hydraulic actuator; optimal controller

1. Introduction

The paper presents how to save the energy demand thanks to the application of smart control system to the multi-dimensional object with multitasking control. In active vibration isolation systems, a reduction of energy demand can be achieved thanks to decreasing requirements to the assumed quality indicators, such as vibration isolation efficiency (passenger comfort) or road holding (safety). The authors of this work proposed the solution that does not decrease the requirements for the assumed quality indicators. It divides control tasks into separate functionalities with its controllers and proposes a superior controller (advanced sliding mode controller (ASMC)) that takes into account the demand for external energy.

In many automobile suspension designs, the body roll is limited by using anti-roll bars. This solution is used in compact vehicles (C-segment), medium vehicles (D-segment), executive cars (E-segment), and also in sports cars (G). The use of controlled vibration reduction systems for the suspension is appropriate in special vehicles where high performance vibration reduction is necessary because of their function, and the costs of manufacturing and operating are offset by the benefits arising from their use. In this paper, the authors focus on finding solutions to both design and control algorithms of special vehicles suspensions (e.g., high-mobility multipurpose wheeled vehicle). The goal of the research was to test a vehicle chassis covering the most commercial technical solutions wheeled vehicle suspension SUV or pickup. The anti-roll bars are rods linking both sides of the suspension, fastened to trailing arms and subjected to torsion when the wheels move in vertical

direction. Their role is to increase the angular rigidity of the front or rear suspension. Using the anti-roll bars allows reducing the body roll when driving on a curve at high speed. The body rolls as a result of centrifugal force acting on it. This force compresses the spring on one side of the car while tensioning the spring on the other side. The bar torsional force reduces the difference in deflection of the suspension springs by increasing the force on the more loaded side (outer wheel) and reducing the force on the less loaded side (inner wheel). A reduced body roll has a positive impact on handling, traction, and grip, thus improving safety. The torsion bars also allow a reduction of roll caused by driving on uneven terrain. During the straight drive on an even surface, at equal excitation of wheels, the stabilizer does not act. When the surface is uneven, the excitation on one wheel will transmit the force to the other wheel via the anti-roll bar, causing an unwanted oscillation. The higher the bar angular rigidity, the more perceptible and uncomfortable this effect will be. Active torsion bars are used to eliminate this effect.

In the field of vehicle roll control, the most popular solutions are the applications of passive torsion bars (or anti-roll bars). The most frequent solutions in the case of controllable systems are an active two-part detachable stabilizer and an active stabilizer. In the two-part detachable stabilizer, the torsion bars are connected or disconnected by means of an actuator. When the wheels operate independently the reaction of one wheel is not transmitted to the other. In the second case, the stabilizer is connected by means of the actuator and acts just like a classic, passive anti-roll bar. The actuator in active anti-roll bar usually is built as a hydraulic controllable clutch which splits the bar into two parts. The pressure value or flow rate control of hydraulic fluid gives various options of influence on the vehicle roll. In the case of active solutions working in vehicles, the energy demand problem is vastly important.

The operational effectiveness of active stabilizers is determined by the control algorithm of the active element (actuator). An increasing amount of attention has been given in recent years to the use of active anti-roll bars in vehicles. The authors of paper [1] used a genetic algorithm to control active anti-roll bars in railway vehicles. As a result, they concluded that it is possible to increase significantly the speed of railway vehicles on fast curves in comparison to vehicles equipped with traditional non-controlled stabilizer bars. The authors of paper [2] presented the analysis of using an active anti-roll bar in off-road vehicles without deterioration of the ride comfort. The paper presents the simulation tests for an off-road vehicle in order to determine the quantitative impact of the active anti-roll bar in terms of both, improving handling and improving ride comfort.

In paper [3] the authors used four independent hydraulic servovalves to control dampers of a model of a heavy vehicle. The authors applied the linear regulator with quadratic performance index (LQR) control algorithm to control the dampers. They compared the operation of a suspension without anti-roll bars, with a system featuring passive anti-roll bars and controlled anti-roll bars proposed by them. The same authors in paper [4] used a robust control algorithm to control active anti-roll bars.

The authors of paper [5] used the sliding mode to control the torque of an active anti-roll bar in a road vehicle. The sliding surface s and limitations for the active roll control system controller are defined as follows in order to reduce the roll angle and relationship between sways.

$$\mathrm{s} = \dot{\phi} + \lambda \cdot \phi,\ s\dot{\mathrm{s}} \leq -\eta|s| \tag{1}$$

Authors of the paper [5] considered only active control of torque in anti-roll bar while the suspension of a vehicle was passive. Additionally, the issue of active suspensions taking into account controlled anti-roll bars were considered [6–13].

In this paper, authors propose the control system of active vehicle suspension which takes into account the task of roll control. The proposed suspension has any anti-roll bar. For this propose, authors use a controller for active independent struts. The motivation for presented research was the initial numerical research presented at the IMAC-XXXVI Conference and Exposition on Structural Dynamics in 2018 [14]. The main tasks of the vehicle suspension control system are to improve the ride quality, handling, road holding, suspension travel, and static deflection [15–22]. Additionally, the roll reduction with

the minimum energetic cost is considered. All these tasks can be achieved by the active vibration control of the vehicle suspension. Synthesis of the multitasks control system for whole suspension is complicated and lead to high-order solutions. The presented method of the controller synthesis takes into account all above mentioned tasks.

The proposed advanced sliding mode controller (ASMC) consist of SMC used to roll reduction and LQRs for struts control was shown. The energy consumption optimization was taken into account at the stage of strut controllers synthesis. Choice of SMC was motivated by many attractive features of this type of control method. One of the most important property is robustness against disturbances. SMC control is a class of variable-structure system. This method instead of the state feedback control law allows switching from one continuous structure to another based on the current position in the state space. The major drawback of SMC method is a risk of occurrence of unwanted high frequency and small amplitude oscillation of control signal known as chattering. This phenomenon makes the control power large or even extremely large [23].

The main advantage of the proposed method is decomposition of the whole vehicle model into two subsystems whose controllers can be chosen independently. The benefit of the proposed approach is the fact that instead of analyzing one high-order problem, two systems of reduced order are analyzed independently. The authors present a mathematical analysis which substantiates the correctness of the proposed method.

The proposed solution consists of two types of controllers arranged in the way that the first SMC controller provides the set point for the second LQR controller. The suspension struts are controlled by hydraulic actuators using controllers whose parameters have been determined with the linear regulator with quadratic performance index (LQR) [24]. These controllers allow a reduction of vertical displacement of the vehicle's geometric center while the SMC is responsible for reducing the body roll. Proposed vehicle model includes dynamics of the actuators. The actuators used for controlling individual suspension struts are hydraulic cylinders with a proportional servovalve. The applied actuator model taking into accounts nonlinearities related to fluid flow through the servovalve ports and the dynamics of the electromechanical transducer. For this reason, the model linearization has been performed in order to synthesize the strut controllers using the LQR method. While the proposed method of SMC synthesis takes into account disturbing inputs in the object model. In the presented example the active suspension of a wheeled vehicle is the object. Disturbances included in the object model are related to the road irregularities the vehicle moves [25]. In the conducted research physical and electrical limitations of the control signals which usually exists in real plants were considered. The simulation tests of the built active suspension control system have been carried out and the results have been shown too. The proposed solution eliminates the need of anti-roll bar usage but thanks to active control the anti-roll function is kept.

2. Active Suspension Model of an SUV Type Vehicle

The discussions presented in the paper are based on the suspension model shown in Figure 1. In the controller synthesis stage, much more simple models are usually used. Applied by the authors controller belongs to the robust category controllers which enable differences between model and the real object. The model applied by authors takes into account the rolling of the vehicle caused by fast cornering but not cover the yaw effect. The authors intend to verify the presented considerations with the use of a real vehicle. The shock absorbers in active struts have been replaced by hydraulic actuators generating forces F_{a_FR} (front right), F_{a_FL} (front left), F_{a_RR} (rear right), F_{a_RL} (rear left). The suspension model accounts for actuators' models with servovalves [26]. Linear springs k_{s_FR}, k_{s_FL}, k_{s_RR}, k_{s_RL} are mounted parallelly to the actuators. It has been assumed that in real hydraulic pistons there are additional damping forces described by c_{s_FR}, c_{s_FL}, c_{s_RR}, c_{s_RL}. The tyres are modelled as elastic elements k_{w_FR}, k_{w_FL}, k_{w_RR}, k_{w_RL} [27,28]. Vertical displacements (**z** axis) of body fastening points to suspension struts are marked as z_{s_FR}, z_{s_FR}, z_{s_RR}, z_{s_RR}. The body rotation angles relative to axes **x**, **y**, and **z** are marked as φ, θ, ψ, respectively. The wheel and tyre mass for individual suspension

struts are modelled as unsprung masses m_{w_FR}, m_{w_FL}, m_{w_RR}, m_{w_RL}. The vertical displacements of those masses are marked z_{w_FR}, z_{w_FL}, z_{w_RR}, z_{w_RL}, respectively. Excitations of suspension struts caused by the road irregularities are modelled as vertical displacements (**z** axis) and are marked $w_{\_FR}$, $w_{\_FL}$, $w_{\_RR}$, $w_{\_RL}$. The vertical displacement of the body center is designated z_s.

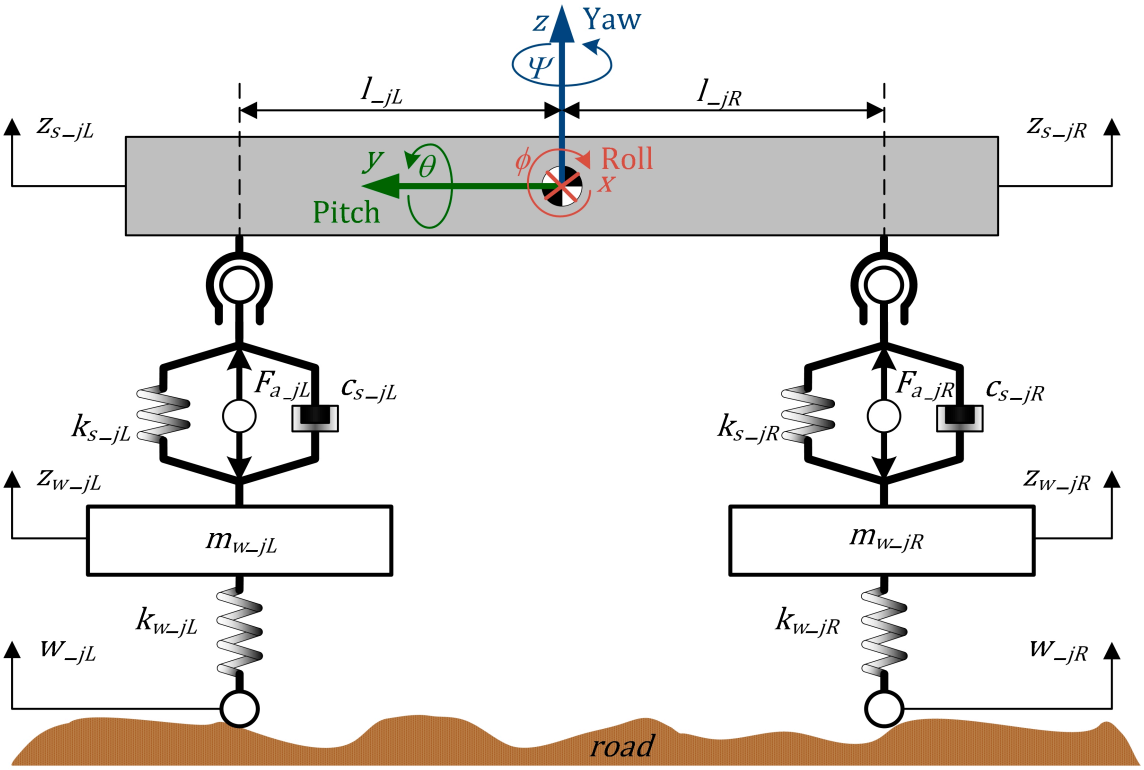

Figure 1. Half vehicle suspension model.

The paper discusses the vehicle body roll (rotation φ around the **x** axis), hence the presented equations and formulas are subscripted $j = F$ for the front suspension and $j = R$ for the rear suspension.

Forces acting on the body car are related to the front suspension struts $\overline{F}_{s\_FR}$ (front right), $\overline{F}_{s\_FL}$ (front left) and the rear suspension struts $\overline{F}_{s\_RR}$ (rear right), $\overline{F}_{s\_RL}$ (rear left), and are expressed by Equations (2) and (3).

$$\overline{F}_{s\_jR} = -k_{s\_jR}\left(z_{s\_jR} - z_{w\_jR}\right) - c_{s\_jR}\left(\dot{z}_{s\_jR} - \dot{z}_{w\_jR}\right) + F_{a\_jR} \tag{2}$$

$$\overline{F}_{s\_jL} = -k_{s\_jL}\left(z_{s\_jL} - z_{w\_jL}\right) - c_{s\_jL}\left(\dot{z}_{s\_jL} - \dot{z}_{w\_jL}\right) + F_{a\_jL} \tag{3}$$

Relationships between displacements z_{s_FR}, z_{s_FR}, z_{s_RR}, z_{s_RR} and the geometric center displacement and rotation angle φ relative to the **x** axis are expressed by Equations (4) and (5).

$$z_{s\_jR} = z_s - \varphi l_{\_jR} \tag{4}$$

$$z_{s\_jL} = z_s + \varphi l_{\_jL} \tag{5}$$

where $l_s = l_{\_jR} = l_{\_jL}$—half car body width.

The suspension analysis has been limited to the chosen front (F) or rear (R) suspension. The equations of motions and moments equilibrium have been formulated only for two suspension struts (front $j = F$ or rear $j = R$).

The car body has been modelled as a rigid body. The equation of forces for the geometric center of the body has been formulated. Only rotation φ relative to the **x** axis has been considered. In this case, only two forces act on the vehicle body: $\overline{F}_{s\_jP}$, $\overline{F}_{s\_jL}$. The force equilibrium equation is as follows (6).

$$m_s\ddot{z}_s = \overline{F}_{s\_jR} + \overline{F}_{s\_jL} \tag{6}$$

where m_s—half body mass.

The moments equilibrium equation relative to the **x** axis is as follows (7).

$$J_s\ddot{\varphi} = -\overline{F}_{s\_jR}l_{\_jR} + \overline{F}_{s\_jL}l_{\_jL} \tag{7}$$

where J_s—half of moment of inertia relative to the vehicle body's **x** axis.

The equations of motions for unsprung masses m_{w_jR}, m_{w_jL} are expressed as follows (8).

$$m_{w\_jR}\ddot{z}_{w\_jR} = -\overline{F}_{s\_jR} - k_{w\_jR}\left(z_{w\_jR} - w_{\_jR}\right) \tag{8}$$

$$m_{w\_jL}\ddot{z}_{w\_jL} = -\overline{F}_{s\_jL} - k_{w\_jL}\left(z_{w\_jL} - w_{\_jL}\right) \tag{9}$$

The actuator assembly with electrohydraulic servovalve for the left and right strut is described with Equations (10), (12), and (13). Variables P_{r_jR}, P_{r_jL} designate the pressure differences in the left and right actuator, respectively. Variables u_{r_jR}, u_{r_jL} designate the displacements of the servovalves' spools. The servovalves' control signals are designated as u_{s_jR}, u_{s_jL}. The model accounts for the suspension deflection ratio ϑ defined as a ratio of relative strut displacement to the suspension vertical deflection. The Equations (10) and (11) are result from the volumetric flow rates equations in the actuator servovalve and account for the hydraulic fluid stiffness [26,29]. The nonlinear phenomenon is usually used in modelling of active hydraulic actuators [30,31]. This model has great importance during fast changes of displacement or force direction and high amplitude of control signal which is often occurring by using SMC methods.

$$\dot{P}_{r\_jR} = u_{r\_jR}l \propto C_d\sqrt{\frac{P_z - P_{r\_jR}\cdot sign\left(u_{r\_jR}\right)}{\rho}} - \propto A_\propto\vartheta\left(\dot{z}_{s\_jR} - \dot{z}_{w\_jR}\right) - \propto C_{tm}P_{r\_jR} \tag{10}$$

$$\dot{P}_{r\_jL} = u_{r\_jL}l \propto C_d\sqrt{\frac{P_z - P_{r\_jL}\cdot sign\left(u_{r\_jL}\right)}{\rho}} - \propto A_\propto\vartheta\left(\dot{z}_{s\_jL} - \dot{z}_{w\_jL}\right) - \propto C_{tm}P_{r\_jL} \tag{11}$$

where $\propto = 44.4495{\cdot}10^{12}\,\frac{N}{m^5}$—hydraulic coefficient,

$l = 15.708{\cdot}10^{-3}$ m—spool valve perimeter,
$C_d = 0.611$ [–]—flow discharge coefficient,
$A_\alpha = 1.09996{\cdot}10^{-3}$ m^2—effective piston area,
$\rho = 880\,\frac{Ns^2}{m^4}$—fluid density, and
$C_{tm} = 0.1{\cdot}10^{-9}\,\frac{m^5}{Ns}$—leakage coefficient.

The servovalve spool dynamics along with an electromechanical transducer is described with the Equations (12) and (13).

$$\tau\dot{u}_{r\_jR} = -u_{r\_jR} + k_{sv}u_{s\_jR} \tag{12}$$

$$\tau\dot{u}_{r\_jL} = -u_{r\_jL} + k_{sv}u_{s\_jL} \tag{13}$$

where $\tau = 2.32{\cdot}10^{-3}$ s—servovalve time constant, and
$k_{sv} = 0.05{\cdot}10^{-3}\,\frac{m}{V}$—voltage to position gain factor.

The forces generated by actuators, taking into account the suspension deflection ratio, are calculated using the following Formulas (14) and (15).

$$F_{a\_jR} = \vartheta A_{\propto} P_{r\_jR} \tag{14}$$

$$F_{a\_jL} = \vartheta A_{\propto} P_{r\_jL} \tag{15}$$

The servovalve control signals u_{s_jR}, u_{s_jL} in a real control system are limited (16).

$$u_{s\_jR} \in [-u_{s\_max}, u_{s\_max}],\ u_{s\_jL} \in [-u_{s\_max}, u_{s\_max}] \tag{16}$$

where u_{s_max}—maximum servovalve control voltage.

The control signals limitations are a significant impediment in the suspension controller synthesis. This stems from the fact that, due to the mechanical and energy limitations, actuators for an active suspension are chosen in such a manner as to minimize their size and power.

3. The ASMC Structure for Active Vehicle Suspension

The task of vibration attenuation by vehicle suspension can be decomposed to the reduction of vibration in the vertical direction and rolling or pitching. The roll vibration frequency is usually up to 4 Hz and is lower than vertical vibration frequency which usually is under 16 Hz. This suggests that during synthesizing the control system these problems should be solved independently. The assumption made during the design of the vehicle active suspension system was that the SMC reduces the roll while the controllers of the individual suspension struts were intended to reduce the vehicle vertical vibration. Such a control system diagram for vehicle's suspension is presented in Figure 2.

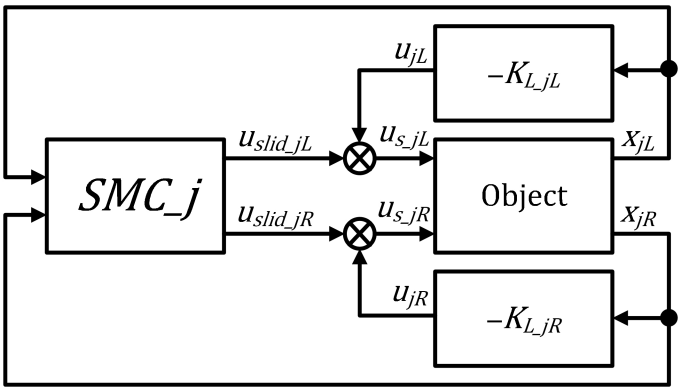

Figure 2. Advanced sliding mode controller (ASMC) block diagram of the system with anti-roll SMC controller and controllers of left and right strut linear regulators with quadratic performance index (LQR).

It has been assumed that controllers K_{L_jR}, K_{L_jL} will be determined independently for each strut and their tasks are to reduce vertical vibration. The SMC has been determined based on the object state Equation (17).

$$\dot{x} = f(x) + B_u(x)u \quad + B_w(x)w \tag{17}$$

where $x \in R^n$—state vector, $u \in R^m$—control signals vector, $w \in R^k$—disturbance vector.

The disturbance signals vector w is related to the excitation caused by the road irregularities and can take away the closed loop system trajectory from the sliding surface.

In the farther part of this section, it was proofed that for bounded disturbance signals it is possible to determine the control for which trajectory of the system moves towards the sliding surface.

The sliding surface is defined by means of the Equation (18).

$$s(x) = 0, s(x) = Cx \tag{18}$$

where $s(x) \in R^m$.

In order to determine the equivalent control u_{eq}, the sliding surface Equation (18) is differentiated with respect to system trajectories (17). As the sliding surface is described with the Equation (18), the equality (19) is satisfied for each moment in time, assuming that $w = 0$.

$$\frac{ds(x(t))}{dt} = 0 \tag{19}$$

Taking into account Equations (17) and (19) we receive the Equation (20).

$$\frac{ds(x(t))}{dt} = \frac{\partial s(x)}{\partial x}\dot{x}(t) = C(f(x(t)) + B_u(x(t))u(t)) \quad = 0 \tag{20}$$

Assuming that the matrix $C{\cdot}B(x)$ is nonsingular, the equivalent control is expressed by the Formula (21).

$$u_{eq} = -(C{\cdot}B_u(x))^{-1}Cf(x) \tag{21}$$

The sliding mode control is then equal to the sum of equivalent control u_{eq} and the control that ensures achieving the sliding surface u_{sw}.

$$u_{slid} = u_{eq} + u_{sw} \tag{22}$$

Method of the control signal u_{sw} determination ensures the system's trajectory convergence to given sliding surface in the presence of disturbance signals w is shown below. The u_{sw} control is chosen in such a manner that $V(x)$ defined with the Formula (23) is a decreasing function along system trajectories (17).

$$V(x) = \frac{1}{2}s^T(x)s(x) \tag{23}$$

The condition (24) must be satisfied then,

$$\frac{d}{dt}V(x(t)) = s^T(x(t))\frac{ds(x(t))}{dt} < 0 \tag{24}$$

Taking into account Formulas (17), (18) and (24) we have received the Formula (25).

$$\frac{d}{dt}V(x(t)) = s^T(x(t))C(f(x(t)) + B_u(x(t))u_{slid}(t) + B_w(x(t))w(t)) \tag{25}$$

Substituting the Formula (21) to the Formula (25) we have received the inequality (26).

$$\frac{d}{dt}V(x(t)) = s^T(x(t))C(B_u(x(t))u_{sw}(t) + B_w(x(t))w(t)) < 0 \tag{26}$$

Vector function $p(t)$ (27) was defined in order to simplify the notation.

$$p(t) = s^T(x(t))CB_u(x(t)) \tag{27}$$

The Formula (26) has then the following form (28).

$$\frac{d}{dt}V(x(t)) = \sum_{i=1}^{m} p_i(t)u_{sw,i}(t) + s^T(x(t))CB_w(x(t))w(t) < 0 \tag{28}$$

This indicates that control signals $u_{sw,i}$ minimizing $\frac{d}{dt}V(x(t))$ can be assumed as follows:

$$u_{sw,i}(t) = \left\{ \begin{array}{cc} -M & for\ p_i(t) > 0 \\ 0 & for\ p_i(t) = 0 \\ M & for\ p_i(t) < 0 \end{array} \right\} \tag{29}$$

Constant $M > 0$ should be chosen in such a manner that condition (24) is satisfied. The first summand in Formula (28) was estimated top-down to this end. As it assumes negative values, in order to estimate is values top-down, its module needs to be estimated bottom-up. The following inequalities take place (30).

$$\left| \sum_{i=1}^{m} p_i(t) u_{sw,i}(t) \right| \geq M \frac{\|p(t)\|}{\sqrt{m}} \geq M \frac{\|(CB_u(x(t)))^{-1}\|_{spec}}{\sqrt{m}} \|s(x)\| \tag{30}$$

The norm $\| \ \|_{spec}$ designates a spectral norm of the matrix (31) (module of maximum eigenvalue for square matrices).

$$\|A\|_{spec} = \sup_{\|x\|=1} \|Ax\| \tag{31}$$

The first inequality in Formula (30) results from the fact that if the vector's Gaussian norm is equal to $\|x\|$, then there is a coordinate of that vector whose module is greater than $\|x\|/\sqrt{m}$, where m is the dimension of the vector space. The second inequality results from the assumption that matrix $CB_u(x)$ is invertible. Equation (30) and the way of choosing signals $u_{sw,i}$ indicate that inequality (32) is satisfied.

$$\sum_{i=1}^{m} p_i(t) u_{sw,i}(t) \leq -M \frac{\|(CB_u(x(t)))^{-1}\|_{spec}}{\sqrt{m}} \|s(x(t))\| \tag{32}$$

The values of the second summand in (28) can be positive or negative and depends on disturbance $w(t)$. This summand was estimated top-down (33).

$$\|s^T(x(t)) CB_w(x(t)) w(t)\| \leq \|s(x(t))\| \cdot \|CB_w(x(t))\| \cdot \|w(t)\| \tag{33}$$

Estimates (32) and (33) indicate that for the condition (24) to be satisfied, the constant M in a certain area of the state space must satisfy the inequality (34).

$$M > \sqrt{m} \frac{\|CB_w(x)\|_{spec}}{\|(CB_u(x))^{-1}\|} \cdot \|w\|_{max} \tag{34}$$

where $\|w\|_{max}$ —maximum from modules of individual coordinates of vector w.

Above considerations prove that for constant M, satisfying inequality (34), the control signal u_{sw} ensures that the system trajectory convergence to the sliding surface. As mentioned before, linear controllers have been determined independently for each of suspension struts using the LQR method. The base for determination of controllers K_{L_jR}, K_{L_jL} is the model in which it was assumed that each strut is loaded with the mass $\frac{1}{2}m_s$, where m_s is a half of the vehicle body mass. Equation (10) describing the servovalve and actuator assembly include a non-linear component described by Formula (35).

$$\Phi\left(P_{r\_jk}, u_{r\_jk}\right) = u_{r\_jk} l \propto C_d \sqrt{\frac{P_z - P_{r\_jk} \cdot sign\left(u_{r\_jk}\right)}{\rho}} \tag{35}$$

where $j \in \{F, R\}$, $k \in \{R, L\}$.

Symbols j, k designate respectively front and rear of a vehicle, and sides left and right (L, R). Function Φ has been approximated with a linear function [29] (36).

$$\Phi\left(P_{r\_jk}, u_{r\_jk}\right) = c_{\Phi,p} P_{r\_jk} + c_{\Phi,u} u_{r\_jk} \tag{36}$$

The coefficients $c_{\Phi,p}$, $c_{\Phi,u}$ of the linear model were determined by means of the least squares method. The model given by Equation (36) was determined for state variables in the operating range [29]. Taking into account the above considerations and Formulas (2) to (36), the equations of the non-linear model for a single suspension strut are

$$\frac{1}{2}m_s\ddot{z}_s = -k_{s\_jk}\left(z_{s\_jk} - z_{w\_jk}\right) - c_{s\_jk}\left(\dot{z}_{s\_jk} - \dot{z}_{w\_jk}\right) + \vartheta A_\propto P_{r\_jk} \tag{37}$$

$$m_{w\_jk}\ddot{z}_{w\_jk} = k_{s\_jk}\left(z_{s\_jk} - z_{w\_jk}\right) + c_{s\_jk}\left(\dot{z}_{s\_jk} - \dot{z}_{w\_jk}\right) - k_{w\_jk}\left(z_{w\_jk} - w_{\_jk}\right) - \vartheta A_\propto P_{r\_jk} \tag{38}$$

$$\dot{P}_{r\_jk} = \left(c_{\Phi,p} - \propto C_{tm}\right)P_{r\_jk} + c_{\Phi,u}u_{r\_jk} - \propto A_\propto \vartheta\left(\dot{z}_{s\_jk} - \dot{z}_{w\_jk}\right) \tag{39}$$

$$\tau\dot{u}_{r\_jk} = -u_{r\_jk} + k_{sv}u_{s\_jk} \tag{40}$$

The following state variables have been used (41)–(43).

$$\overline{x}_{jk} = \left(z_{s\_jk}, \dot{z}_{s\_jk}, z_{w\_jk}, \dot{z}_{w\_jk}, P_{r\_jk}, u_{r\_jk}\right)^T \tag{41}$$

$$u_{jk} = u_{s\_jk} \tag{42}$$

$$w_{jk} = w_{\_jk} \tag{43}$$

The state equations describing a suspension strut are as follows (44).

$$\frac{d\overline{x}_{jk}}{dt} = A_{jk}\overline{x}_{jk} + B_{u\_jk}u_{jk} + B_{w\_jk}\,w_{jk} \tag{44}$$

In order to synthesize the state controller with the LQR method, it has been assumed that $w_{jk} = 0$. The quality indicator has then the form (45).

$$J = \int_0^\infty x_{jk}^T Q_{jk}\overline{x}_{jk} + u_{jk}^T R_{jk}u_{jk}dt \tag{45}$$

where matrices Q_{jk}, R_{jk}—symmetrical positive definite matrices.

The Riccati Equation (46) must be solved in order to determine the controller.

$$P_{jk}A_{jk} + A_{jk}^T P_{jk} - P_{jk}B_{jk}R_{jk}^{-1}B_{jk}^T P_{jk} + Q_{jk} = 0 \tag{46}$$

The state controller K_{L_jk} is determined according to the Formula (47).

$$K_{L\_jk} = R_{jk}^{-1}B_{jk}^T P_{jk} \tag{47}$$

The control signal is then described with the Formula (48).

$$u_{jk} = -K_{L\_jk}\overline{x}_{jk} \tag{48}$$

The parameters of front and rear suspension struts in road vehicles are usually different nevertheless the struts used in front or rear suspension are identical. Their parameters may differ slightly due to variability of components caused by the production process, or possibly uneven wear. For this reason, the following designations (49)–(53) have been assumed in the further part of the paper. It was assumed that center of the mass coincides with geometric center of the car body. The body mass center of the real vehicle is not in its geometric center moreover, its position may change and depends on the load distribution. This problem was solved by application the sliding controller (SMC) which generates an appropriate correction signal.

$$k_{s\_j} = k_{s\_jR} = k_{s\_jL} \tag{49}$$

$$c_{s\_j} = c_{s\_jR} = c_{s\_jL} \tag{50}$$

$$k_{w\_j} = k_{w\_jR} = k_{w\_jL} \tag{51}$$

$$m_{w\_j} = m_{w\_jR} = m_{w\_jL} \tag{52}$$

$$l_s = l_{\_jR} = l_{\_jL} \tag{53}$$

The suspensions struts controllers have been synthesized for an SUV. The following suspension parameters have been assumed: $m_w = 35.5$ kg, $k_w = 100\ \frac{\text{kN}}{\text{m}}$, $\frac{1}{4}m_s = 365$ kg, $k_s = 20\ \frac{\text{kN}}{\text{m}}$, $c_s = 1290\ \frac{\text{Ns}}{\text{m}}$. Due to mechanical and energy limitations, the assumption has been made that a displacement vibration transfer function should be less than −18 dB over the entire frequency range. The following values of weight matrices Q, R were assumed in the quality indicator (45).

$$Q_{jk} = \left\{ \begin{array}{cc} 1 & for\ k = \text{L},\ \text{j} \in \{F, R\} \\ 2E-3 & for\ k = R,\ \text{j} \in \{F, R\} \\ 0 & in\ other\ cases \end{array} \right\},\ R_{jk} = 4 \times 10^{-8} \tag{54}$$

Figure 3 presents the obtained vibration transmissibility functions Tzs, w (55), (56) for a vehicle suspension strut. The function has been determined based on the model of a linearized actuator assembly.

$$Tz_{s\_jk}, w_{\_jk} = 10log\left(\frac{\int_0^{T_f} z_{s\_jk}^2 dt}{\int_0^{T_f} w_{\_jk}^2 dt} \right) \tag{55}$$

$$Tzs, w = Tz_{s\_jR}, w_{\_jR} = Tz_{s\_jL}, w_{\_jL} \tag{56}$$

where T_f—is period of excitation signal, z_{s_jk} and $w_{\_jk}$ are function of frequency; constant value was removed from both signals.

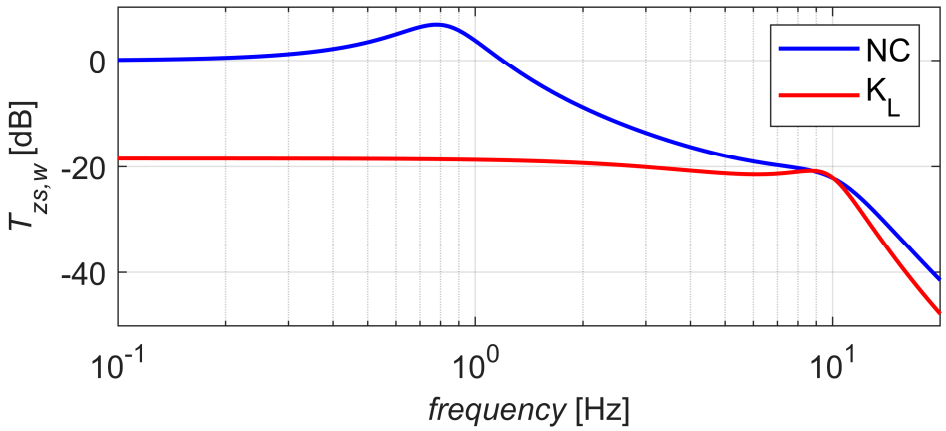

Figure 3. Vibration transmissibility functions for a suspension strut with no controller (NC) and state controller (K_L).

The coefficients in the Formula (36) were $c_{\Phi,p} = -341.2$, $c_{\Phi,u} = 4.66 \times 10^{13}$ Analyzing Figure 3, it can be noticed that above 1.4 Hz the vibration transfer function has values below −20 dB. This indicates that the vehicle roll reduction should be most effective in the range up to 4 Hz.

4. Synthesis of the SMC

As mentioned above, the role of SMC is to reduce the vehicle body roll. The basis for the synthesis of the SMC is a suspension half-model with struts controlled by controllers K_{L_jR}, K_{L_jL} determined in the previous section. The disturbances appear as an uncertainty of the model parameters or other

imperfections in the models used to design the feedback law. Taking into account the fact that the suspension struts are identical for certain rear or front half car—Equations (4), (5) and (49)–(53) together with the Equations (57) and (58) for differences and sums of variables z_{s_jR}, z_{w_jL} have been obtained.

$$z_{s\_jL} - z_{s_{jR}} = -z_s + \varphi l_s + z_s + \varphi l_s = 2\varphi l_s \tag{57}$$

$$z_{s\_jR} + z_{s\_jL} = z_s - \varphi l_s + z_s + \varphi l_s = 2z_s \tag{58}$$

This equation describing the motion of the body geometric center includes a component which is a sum of forces $\overline{F}_{s\_jR}$, $\overline{F}_{s\_jL}$. The sum (59) of these forces has been determined taking into account Formulas (2), (49)–(53), (57), and (58).

$$\begin{array}{l} \overline{F}_{s\_jR} + \overline{F}_{s\_jL} = -k_{s\_j}\left(z_{s\_jR} - z_{w\_jR}\right) - c_{s\_j}\left(\dot{z}_{s\_jR} - \dot{z}_{w\_jR}\right) + F_{a\_jR} \\ -k_{s\_j}\left(z_{s\_jL} - z_{w\_jL}\right) - c_{s\_j}\left(\dot{z}_{s\_jL} - \dot{z}_{w\_jL}\right) + F_{a\_jL} = \\ -2k_{s\_j}z_s + k_{s\_j}\left(z_{w\_jR} + z_{w\_jL}\right) - 2c_{s\_j}\dot{z}_s + c_{s\_j}\left(\dot{z}_{w\_jR} + \dot{z}_{w\_jL}\right) + \vartheta A_\propto\left(P_{r\_jR} + P_{r\_jL}\right) \end{array} \tag{59}$$

Similarly, the equation describing the body rotation includes a component which is a difference of forces $\overline{F}_{s\_jR}$, $\overline{F}_{s\_jL}$. The difference (60) of these forces has been determined taking into account Formulas (2), (49)–(53), (57), and (58).

$$\begin{array}{l} -\overline{F}_{s\_jR} + \overline{F}_{s\_jL} = k_{s\_j}\left(z_{s\_jR} - z_{w\_jR}\right) + c_{s\_j}\left(\dot{z}_{s\_jR} - \dot{z}_{w\_jR}\right) - F_{a\_jR} \\ -k_{s\_j}\left(z_{s\_jL} - z_{w\_jL}\right) - c_{s\_j}\left(\dot{z}_{s\_jL} - \dot{z}_{w\_jL}\right) + F_{a\_jL} = \\ -2k_{s\_j}\, l_s\varphi - k_{s\_j}\left(z_{w\_jR} - z_{w\_jL}\right) - 2c_{s\_j}\, l_s\dot{\varphi} - c_{s\_j}\left(\dot{z}_{w\_jR} - \dot{z}_{w\_jL}\right) - \vartheta A_\propto\left(P_{r\_jR} - P_{r\_jL}\right) \end{array} \tag{60}$$

As the left and right strut are identical, the controllers K_{L_jR}, K_{L_jL} determined in the previous section are also identical.

$$K_{L\_j} = K_{L\_jR} = K_{L\_jL} \tag{61}$$

$$z_{s\_jR} + z_{w\_jL} = z_s - \varphi l_s + z_s + \varphi l_s = 2z_s \tag{62}$$

The suspension half-model takes into account controllers for each of struts. The model consists of four sets of differential equations describing: the motion of the vehicle geometric center (63), rotation around the x axis (64), the right and left struts dynamics (65) to (70). The Equation (63) describing the motion of the vehicle geometric center have been determined based on Equations (6) and (59).

$$m_s\ddot{z}_s = -2k_{s\_j}z_s + k_{s\_j}\left(z_{w\_jR} + z_{w\_jL}\right) - 2c_{s\_j}\dot{z}_s + c_{s\_j}\left(\dot{z}_{w\_jR} + \dot{z}_{w\_jL}\right) + \vartheta A_\propto\left(P_{r\_jR} + P_{r\_jL}\right) \tag{63}$$

The Equation (64) describing rotation φ around the vehicle body's **x** axis have been determined based on Equations (7) and (60).

$$\begin{array}{l} J_s\ddot{\varphi} = -2k_{s\_j}l_s^2\varphi - k_{s\_j}l_s\left(z_{w\_jR} - z_{w\_jL}\right) - 2c_{s\_j}l_s^2\dot{\varphi} - c_{s\_j}l_s\left(\dot{z}_{w\_jR} - \dot{z}_{w\_jL}\right) \\ -\vartheta A_\propto l_s\left(P_{r\_jR} - P_{r\_jL}\right) \end{array} \tag{64}$$

Taking into account Formulas (10), (12), (13), (57), and (58) we have received the equations describing the right (65)–(67) and the left suspension strut (68)–(70).

$$m_{w\_j}\ddot{z}_{w\_jR} = k_{s\_j}\left(z_s - \varphi l_s - z_{w\_jR}\right) + c_{s\_j}\left(\dot{z}_s - \dot{\varphi} l_s - \dot{z}_{w\_jR}\right) - k_{w\_j}\left(z_{w\_jR} - w_{\_jR}\right) - \vartheta A_\propto P_{r\_jR} \tag{65}$$

$$\dot{P}_{r\_jR} = u_{r\_jR}l \propto C_d\sqrt{\frac{P_z - P_{r\_jR}\cdot sign\left(u_{r\_jR}\right)}{\rho}} - \propto A_\propto\vartheta\left(\dot{z}_s - \dot{\varphi} l_s - \dot{z}_{w\_jR}\right) - \propto C_{tm}P_{r\_jR} \tag{66}$$

$$\tau\dot{u}_{r\_jR} = -u_{r\_jR} - k_{sv}K_{L\_j}\overline{x}_{jR} + k_{sv}u_{slid\_jR} \tag{67}$$

The left suspension strut has been described with Equations (68)–(70)

$$m_{w\_j}\ddot{z}_{w\_jL} = k_{s\_j}\left(z_s + \varphi l_s - z_{w\_jL}\right) + c_{s\_j}\left(\dot{z}_s + \dot{\varphi} l_s - \dot{z}_{w\_jR}\right) - k_{w\_j}\left(z_{w\_jL} - w_{\_jL}\right) - \vartheta A_{\propto} P_{r\_jL} \tag{68}$$

$$\dot{P}_{r\_jL} = u_{r\_jL} l \propto C_d \sqrt{\frac{P_z - P_{r\_jL} \cdot sign\left(u_{r\_jL}\right)}{\rho}} - \propto A_{\propto} \vartheta\left(\dot{z}_s + \dot{\varphi} l_s - \dot{z}_{w\_jL}\right) - \propto C_{tm} P_{r\_jL} \tag{69}$$

$$\tau \dot{u}_{r\_jL} = -u_{r\_jL} - k_{sv} K_{L\_j} \overline{x}_{jL} + k_{sv} u_{slid\_jL} \tag{70}$$

The analysis of the equation system (63)–(70) describing the suspension model indicates that the whole vehicle model can be decomposed into the following independent subsystems: model describing the motion of vehicle geometric center (91)–(94), and the model describing the rotation around the x axis (87) to (90) and (89). In case of the linearized Equations (65)–(70) models described by (87)–(94) equations are independent of each other. The following transformation of variables has been performed in order to prove this thesis (71)–(76).

$$z^{+}_{w\_j} = \frac{1}{2}\left(z_{w\_jR} + z_{w\_jL}\right),\ z^{-}_{w\_j} = \frac{1}{2}\left(-z_{w\_jR} + z_{w\_jL}\right) \tag{71}$$

$$P^{+}_{r\_j} = \frac{1}{2}\left(P_{r\_jR} + P_{r\_jL}\right),\ P^{-}_{r\_j} = \frac{1}{2}\left(-P_{r\_jR} + P_{r\_jL}\right) \tag{72}$$

$$u^{+}_{r\_j} = \frac{1}{2}\left(u_{r\_jR} + u_{r\_jL}\right),\ u^{-}_{r\_j} = \frac{1}{2}\left(-u_{r\_jR} + u_{r\_jL}\right) \tag{73}$$

$$u^{+}_{slid\_j} = \frac{1}{2}\left(u_{slid\_jR} + u_{slid\_jL}\right),\ u^{-}_{slid\_j} = \frac{1}{2}\left(-u_{slid\_jR} + u_{slid\_jL}\right) \tag{74}$$

$$w^{+}_{\_j} = \frac{1}{2}\left(w_{\_jR} + w_{\_jL}\right),\ w^{-}_{\_j} = \frac{1}{2}\left(-w_{\_jR} + w_{\_jL}\right) \tag{75}$$

$$\overline{x}^{+}_{\_j} = \frac{1}{2}\left(\overline{x}_{jR} + \overline{x}_{jL}\right),\ \overline{x}^{-}_{\_j} = \frac{1}{2}\left(-\overline{x}_{jR} + \overline{x}_{jL}\right) \tag{76}$$

This is the authors' idea that it is possible to reduce the order of the model by half. Such a notation for a linear model enables the controller synthesis for the reduced order of the model and the subsequent decomposition of the control for the equations with the sign "+" and "−". The variables with the "+" sign are used in modelling vertical vibration and that signed "−" are used for rolling modelling. These models would be independent of each other but the nonlinear part raises doubts connected to the model accuracy. However, it can be compensated by using the SMC method which is robust for some model deviation. That is why the independent controller's synthesis for vibration and roll reductions is possible.

Vectors $\overline{x}^{+}_{\_j}$, $\overline{x}^{-}_{\_j}$ (77), (78) have been determined by substituting Formulas (57) and (58) to Equations (71) to (76).

$$\overline{x}^{+}_{\_j} = \left(z_s, \dot{z}_s, z^{+}_{w\_j}, \dot{z}^{+}_{w\_j}, P^{+}_{r\_j}, u^{+}_{r\_j}\right)^T \tag{77}$$

$$\overline{x}^{-}_{\_j} = \left(\varphi, \dot{\varphi}, z^{-}_{w\_j}, \dot{z}^{-}_{w\_j}, P^{-}_{r\_j}, u^{-}_{r\_j}\right)^T \tag{78}$$

Vector $\overline{x}^{+}_{\_j}$ comprises variables with plus superscript as well as variables z_s, and $\dot{z}_s$, whereas vector $\overline{x}^{-}_{\_j}$ comprises variables with minus superscript as well as variables φ and $\dot{\varphi}$. By differentiating the variables described by Formulas (71)–(76) and taking into account the models described by Equations (57) and (58) we have received the models described with Equations (79)–(86). The vehicle roll is described by the model (79)–(82).

$$J_s \ddot{\varphi} = -2k_{s\_j} l_s^2 \varphi + 2k_{s\_j} l_s z^{-}_{w\_j} - 2c_{s\_j} l_s^2 \dot{\varphi} + c_{s\_j} l_s \dot{z}^{-}_{w\_j} + \vartheta A_{\propto} l_s P^{-}_{r\_j} \tag{79}$$

$$m_{w\_j}\ddot{z}^{-}_{w\_j} = k_{s\_j}\left(\varphi l_s - z^{-}_{w\_j}\right) + c_{s\_j}\left(\dot{\varphi} l_s - \dot{z}^{-}_{w\_j}\right) - k_{w\_j}\left(z^{-}_{w\_j} - w^{-}_{\_j}\right) - \vartheta A_{\propto} P^{-}_{r\_j} \tag{80}$$

$$\begin{aligned} 2\dot{P}^{+}_{r\_j} = \left(u^{+}_{r\_j} + u^{-}_{r\_j}\right) l \propto C_d \sqrt{\frac{P_z - \left(P^{+}_{r\_j} + P^{-}_{r\_j}\right)\cdot sign\left(u^{+}_{r\_j} + u^{-}_{r\_j}\right)}{\rho}} + \\ -\left(u^{+}_{r\_j} - u^{-}_{r\_j}\right) l \propto C_d \sqrt{\frac{P_z - \left(P^{+}_{r\_j} - P^{-}_{r\_j}\right)\cdot sign\left(u^{+}_{r\_j} - u^{-}_{r\_j}\right)}{\rho}} \\ -2 \propto A_{\propto}\vartheta\left(\dot{\varphi} l_s - \dot{z}^{-}_{w\_j}\right) - 2 \propto C_{tm} P^{-}_{r\_j} \end{aligned} \tag{81}$$

$$\tau \dot{u}^{-}_{r\_j} = -u^{-}_{r\_j} - k_{sv} K_{L\_j} \bar{x}^{-}_{\_j} + k_{sv} u^{-}_{slid\_j} \tag{82}$$

Model (83)–(86) allows determination of the vertical displacement of the vehicle geometric center.

$$m_s \ddot{z}_s = -2k_{s\_j} z_s + 2k_{s\_j} z^{+}_{w\_j} - 2c_{s\_j}\dot{z}_s + 2c_{s\_j}\dot{z}^{+}_{w\_j} + 2\vartheta A_{\propto} P^{+}_{r\_j} \tag{83}$$

$$m_{w\_j}\ddot{z}^{+}_{w\_j} = k_{s\_j}\left(z_s - z^{+}_{w\_j}\right) + c_{s\_j}\left(\dot{z}_s - \dot{z}^{+}_{w\_j}\right) - k_{w\_j}\left(z^{+}_{w\_j} - w^{+}_{\_j}\right) - \vartheta A_{\propto} P^{+}_{r\_j} \tag{84}$$

$$\begin{aligned} \dot{P}^{+}_{r\_j} = \tfrac{1}{2}\Bigg[\left(u^{+}_{r\_j} + u^{-}_{r\_j}\right) l \propto C_d \sqrt{\frac{P_z - \left(P^{+}_{r\_j} + P^{-}_{r\_j}\right)\cdot sign\left(u^{+}_{r\_j} + u^{-}_{r\_j}\right)}{\rho}} + \\ +\left(u^{+}_{r\_j} - u^{-}_{r\_j}\right) l \propto C_d \sqrt{\frac{P_z - \left(P^{+}_{r\_j} - P^{-}_{r\_j}\right)\cdot sign\left(u^{+}_{r\_j} - u^{-}_{r\_j}\right)}{\rho}}\Bigg] \\ - \propto A_{\propto}\vartheta\left(\dot{z}_s - \dot{z}^{+}_{w\_j}\right) - \propto C_{tm} P^{+}_{r\_j} \end{aligned} \tag{85}$$

$$\tau \dot{u}^{+}_{r\_j} = -u^{+}_{r\_j} - k_{sv} K_{L\_j} \bar{x}^{+}_{\_j} + k_{sv} u^{+}_{slid\_j} \tag{86}$$

The state variables appearing in both models are related to the displacements of the spool and pressure differences in servovalves. They appear simultaneously only in the equation related to the pressure difference derivative. Taking into account the Formula (36), the models (79)–(86) have been linearized and as a result, two independent models have been obtained. The model (87)–(90) describes the vehicle roll and depends only on state variables with minus superscript and variables φ, $\dot{\varphi}$.

$$J_s \ddot{\varphi} = -2k_{s\_j} l_s^2 \varphi + 2k_{s\_j} l_s z^{-}_{w\_j} - 2c_{s\_j} l_s^2 \dot{\varphi} + c_{s\_j} l_s \dot{z}^{-}_{w\_j} + \vartheta A_{\propto} l_s P^{-}_{r\_j} \tag{87}$$

$$m_{w\_j}\ddot{z}^{-}_{w\_j} = k_{s\_j}\left(\varphi l_s - z^{-}_{w\_j}\right) + c_{s\_j}\left(\dot{\varphi} l_s - \dot{z}^{-}_{w\_j}\right) - k_{w\_j}\left(z^{-}_{w\_j} - w^{-}_{\_j}\right) - \vartheta A_{\propto} P^{-}_{r\_j} \tag{88}$$

$$\dot{P}^{-}_{r\_j} = - \propto A_{\propto}\vartheta\left(\dot{\varphi} l_s - \dot{z}^{-}_{w\_j}\right) - \left(c_{\Phi,p} - \propto C_{tm}\right) P^{-}_{r\_j} + c_{\Phi,u} u^{-}_{r\_j} \tag{89}$$

$$\tau \dot{u}^{-}_{r\_j} = -u^{-}_{r\_j} - k_{sv} K_{L\_j} \bar{x}^{-}_{\_j} + k_{sv} u^{-}_{slid\_j} \tag{90}$$

The vehicle vertical displacements are described by the model (91)–(94) and depend on state variables with plus superscript and variables z_s, $\dot{z}_s$.

$$m_s \ddot{z}_s = -2k_{s\_j} z_s + 2k_{s\_j} z^{+}_{w\_j} - 2c_{s\_j}\dot{z}_s + 2c_{s\_j}\dot{z}^{+}_{w\_j} + 2\vartheta A_{\propto} P^{+}_{r\_j} \tag{91}$$

$$m_{w\_j}\ddot{z}^{+}_{w\_j} = k_{s\_j}\left(z_s - z^{+}_{w\_j}\right) + c_{s\_j}\left(\dot{z}_s - \dot{z}^{+}_{w\_j}\right) - k_{w\_j}\left(z^{+}_{w\_j} - w^{+}_{\_j}\right) - \vartheta A_{\propto} P^{+}_{r\_j} \tag{92}$$

$$\dot{P}^{+}_{r\_j} = - \propto A_{\propto}\vartheta\left(\dot{z}_s - \dot{z}^{+}_{w\_j}\right) + \left(c_{\Phi,p} - \propto C_{tm}\right) P^{+}_{r\_j} + c_{\Phi,u} u^{+}_{r\_j} \tag{93}$$

$$\tau \dot{u}^{+}_{r\_j} = -u^{+}_{r\_j} - k_{sv} K_{L\_j} \bar{x}^{+}_{\_j} + k_{sv} u^{+}_{slid\_j} \tag{94}$$

This discussion indicates that the design of SMC for reduction of vehicle body roll can be limited to state variables appearing in the models (87)–(90). The equation of sliding surface s can be then described with the Equation (95).

$$s = c_1\varphi + c_2\dot{\varphi} + c_3 z^-_{w\_j} + c_4 \dot{z}^-_{w\_j} + c_5 P^-_{r\_j} + c_6 u^-_{r\_j} \tag{95}$$

As the coefficient of the variable $u^-_{r\_j}$ in Equation (95) after taking into account the assumption of Equation (21) solutions existence the c_6 must be different than zero, without loss of generality it can be assumed that c_6 is equal to one. The following state variables describing the vehicle active suspension have been assumed.

$$x^- = \left(\varphi, \dot{\varphi}, z^-_{w\_j}, \dot{z}^-_{w\_j}, P^-_{r\_j}, u^-_{r\_j}\right)^T,\ x^+ = \left(z_s, \dot{z}_s, z^+_{w\_j}, \dot{z}^+_{w\_j}, P^+_{r\_j}, u^+_{r\_j}\right)^T \tag{96}$$

The function describing the object dynamics and vehicle roll has been designated as $f^-(x^-, x^+)$ and is expressed with Equation (97).

$$\begin{gathered} f^-(x^-, x^+) = \begin{pmatrix} x^-_2 \\ \frac{-2k_{s\_j}l_s^2 x^-_1 - 2c_{s\_j}l_s^2 x^-_2 + 2k_{s\_j}l_s x^-_3 + c_{s\_j}l_s x^-_4 + \vartheta A_\propto l_s x^-_5}{J_s} \\ x^-_4 \\ \frac{k_{s\_j}l_s x^-_1 + c_{s\_j}l_s x^-_2 - \left(k_{s\_j}+k_{w\_j}\right)x^-_3 - c_{s\_j}x^-_4 - \vartheta A_\propto x^-_5}{m_{w\_j}} \\ -2 \propto A_\propto \vartheta l_s x^-_2 + 2 \propto A_\propto \vartheta x^-_4 - 2 \propto C_{tm} x^-_5 + \\ \frac{1}{2}\left(x^+_6 + x^-_6\right) l \propto C_d \sqrt{\frac{P_z - \left(x^+_5 + x^-_5\right)\cdot sign\left(x^+_6 + x^-_6\right)}{\rho}} - \\ -\frac{1}{2}\left(x^+_6 - x^-_6\right) l \propto C_d \sqrt{\frac{P_z - \left(x^+_5 - x^-_5\right)\cdot sign\left(x^+_6 - x^-_6\right)}{\rho}} \\ \frac{-u^-_{r\_j} - k_{sv}K_{L\_j}\bar{x}^-_{\_j}}{\tau} \end{pmatrix} \\ B^-_u = \left(0,0,0,0,0,\frac{k_{sv}}{\tau}\right)^T,\ B^-_w = \left(0,0,0,\frac{k_{w\_j}}{m_{w\_j}},0,0\right)^T \end{gathered} \tag{97}$$

The function describing the vertical displacement of geometric center has been designated as $f^+(x^-, x^+)$ and is expressed with Equation (98).

$$\begin{gathered} f^+(x^-, x^+) = \begin{pmatrix} x^+_2 \\ \frac{-2k_{s\_j}x^+_1 - 2c_{s\_j}x^+_2 + 2k_{s\_j}x^+_3 + 2c_{s\_j}x^+_4 + 2\vartheta A_\propto x^+_5}{m_s} \\ x^+_4 \\ \frac{k_{s\_j}l_s x^+_1 + c_{s\_j}l_s x^+_2 - \left(k_{s\_j}+k_{w\_j}\right)x^+_3 - c_{s\_j}x^+_4 - \vartheta A_\propto x^+_5}{m_{w_j}} \\ -2 \propto A_\propto \vartheta l_s x^+_2 + 2 \propto A_\propto \vartheta x^+_4 - 2 \propto C_{tm} x^+_5 + \\ \frac{1}{2}\left(x^+_6 + x^-_6\right) l \propto C_d \sqrt{\frac{P_z - \left(x^+_5 + x^-_5\right)\cdot sign\left(x^+_6 + x^-_6\right)}{\rho}} - \\ +\frac{1}{2}\left(x^+_6 - x^-_6\right) l \propto C_d \sqrt{\frac{P_z - \left(x^+_5 - x^-_5\right)\cdot sign\left(x^+_6 - x^-_6\right)}{\rho}} \\ \frac{-u^+_{r\_j} - k_{sv}K_{L\_j}\bar{x}^+_{\_j}}{\tau} \end{pmatrix} \\ B^+_u = \left(0,0,0,0,0,\frac{k_{sv}}{\tau}\right)^T,\ B^+_w = \left(0,0,0,\frac{k_{w\_j}}{m_{w\_j}},0,0\right)^T \end{gathered} \tag{98}$$

The model describing the road vehicle suspension takes the following form (99) and (100).

$$\dot{x}^- = f^-(x^-, x^+) + B^-_u u^-_{slid\_j} + B^-_w w^-_{\_j} \tag{99}$$

$$\dot{x}^{+} = f^{+}\left(x^{-}, x^{+}\right) + B_{u}^{+} u_{slid\_j}^{+} + B_{w}^{+} w_{\_j}^{+} \tag{100}$$

The model takes into account the controller included in individual suspension strut. The sliding surface is then described with the formula,

$$s(x^{-}) = cx^{-} \tag{101}$$

Because the assumption has been made that the role of the SMC is to reduce the roll, it can be assumed that $u_{slid\_j}^{+} = 0$. Then the equivalent control is determined based on the Formula (21) and expressed with the Formulas (102) and (103).

$$u_{eq\_slid\_j}^{-} = -\frac{\tau}{k_{sv}} c f^{-}(x^{-}, x^{+}) \tag{102}$$

$$u_{eq\_slid\_j}^{+} = 0 \tag{103}$$

Taking into account the Formulas (102) and (103), the following formula for sliding mode control was assumed for (104) and (105),

$$u_{sw\_slid\_j}^{-} = u_{eq\_slid\_j}^{-} - Msign(s(x^{-})) \tag{104}$$

$$u_{sw\_slid\_j}^{+} = 0 \tag{105}$$

Taking into account the Formulas (71)–(76), (104), and (105) the control signals applied to the right and left suspension struts are expressed with Formulas (106) and (107).

$$u_{slid\_jR} = -0.5\left(\frac{\tau}{k_{sv}} c f^{-}(x^{-}, x^{+}) + Msign(s(x^{-}))\right) \tag{106}$$

$$u_{slid\_jL} = 0.5\left(\frac{\tau}{k_{sv}} c f^{-}\left(x^{-}, x^{+}\right) + Msign(s(x^{-}))\right) \tag{107}$$

Taking into account the Formulas (65)–(70), (106), and (107), limitations for the servovalves control signals, these signals are expressed with Formulas (108)–(109).

$$u_{s\_jR} = sat\left(-K_{L\_j}\bar{x}_{jR} - 0.5\left(\frac{\tau}{k_{sv}} c f^{-}(x^{-}, x^{+}) + Msign(s(x^{-}))\right)\right) \tag{108}$$

$$u_{s\_jL} = sat\left(-K_{L\_j}\bar{x}_{jL} + 0.5\left(\frac{\tau}{k_{sv}} c f^{-}\left(x^{-}, x^{+}\right) + Msign(s(x^{-}))\right)\right) \tag{109}$$

where $M \in [-u_{s\_max}, u_{s\_max}]$.

Function $sat(u)$ is defined by the Formula (110).

$$sat(u) = \left\{ \begin{array}{cc} u_{s\_max} & dla\ u > u_{s\_max} \\ u & dla\ u \in [-u_{s\_max}, u_{s\_max}] \\ -u_{s\_max} & dla\ u < -u_{s\_max} \end{array} \right\} \tag{110}$$

The limitations for the servovalves control signals u_{s_jP}, u_{s_jL} could be the reason of leaving the sliding surface. Such a situation occurs for large amplitudes or high frequencies of exciting signals. The vehicle suspension analysis indicates that the greatest vehicle roll values will occur for exciting signals acting on the left $w_{\_jL}$ and the right $w_{\_jR}$ strut shifted by $\pi/2$.

5. Numerical Research of the ASMC Control System

The simulation tests were carried out in order to verify the proposed synthesis method of the SMC. The simulations were carried out by using software-in-Loop (SIL) methods. Numerical research was carried out with a constant sample rate equaled 1 ms. The control signal output was limited to real hardware range (±10V). The model used for tests was verified with the real wheeled vehicle. The selected

tests are presented below. In these tests, a nonlinear model of the actuator was considered in the suspension model. The following sliding surface parameters were used: (95) $c_1 = 0.8$; $c_3 = c_4 = c_5 = 0$. The constant M in Formula (29) is 2 V. On all presented figures the exciting signals in the meaning of disturbance $w_{\_jR}$, $w_{\_jL}$ applied to suspension struts are shifted in phase.

$$w_{\_jL} = A_{w\_jL} sin\left(2\pi f_{w\_jL} t\right) \tag{111}$$

$$w_{\_jR} = A_{w\_jR} sin\left(2\pi f_{w\_jR} t + \frac{\pi}{2}\right) \tag{112}$$

Figures 4, 5 and 6a present the time courses of signals which are responses to the exciting signals Figure 6b. Amplitudes and frequencies of excitation signals were 0.01 m and 2 Hz, respectively. The phase shift between signals was established on $\frac{\pi}{2}$ Figure 6b.

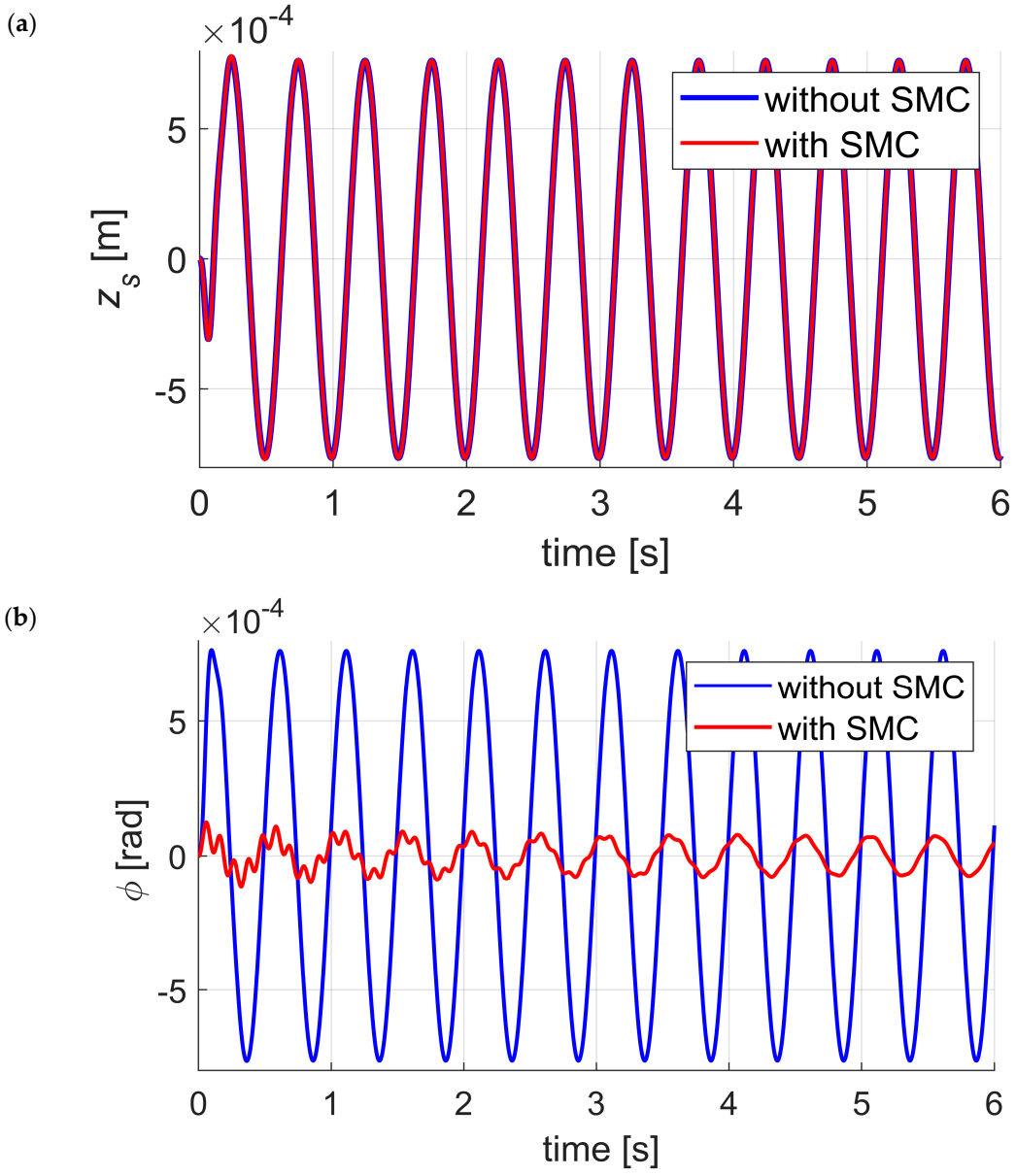

Figure 4. Time courses of the: vertical displacement z_s (**a**), and roll angle φ (**b**) for$A_{w_jR} = A_{w_jL} =$ 0.01 m, $f_{w\_jR} = f_{w\_jL} = 2$ Hz.

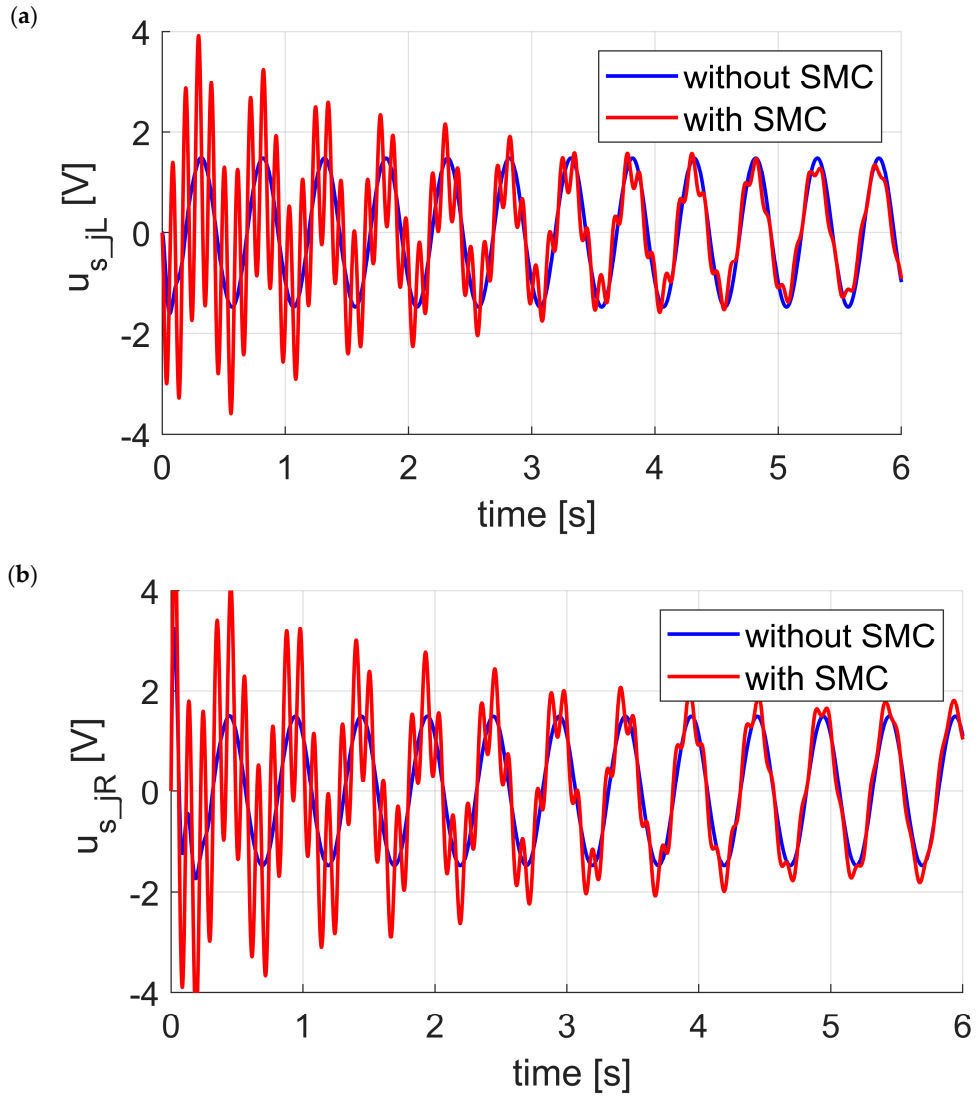

Figure 5. Comparison of struts control signals with and without SMC for left strut (**a**) and right strut (**b**) for $A_{w\_jR} = A_{w\_jL} = 0.01$ m, $f_{w\_jR} = f_{w\_jL} = 2$ Hz.

As one can see in Figure 4a designed SMC is not dedicated to reducing vertical vibration—presented curves coincide. The amplitude of variable φ (vehicle roll) without SMC was 0.0096 rad, and with SMC was reduced to 0.00075 rad (Figure 4b). LQR controllers related to individual struts were active in both cases. LQR controllers of individual struts ensure the reduction of vertical vibration while at the same time minimal energy requirement is demanded. This requirement can be seen on quality indicator (34). The use of SMC in the addition control layer allowed the roll to be reduced 12 times for the 2 Hz exciting signals. The efficiency of roll reduction is defined by the selection of sliding surface parameters. Figure 5 presents the control signals for the left and right strut (including the signals generated by the LQR controllers). Control signals are within the permitted range from −10 V to 10 V. Analyzing Figure 5a,b it can be noticed that the control signals are distorted, and their values decrease with the system approaching the sliding manifold in the case of working SMC.

Figure 6a presents the control signals generated by the SMC. The control signals for the left and right strut (106) and (107) differ only in the sign. Just like previously, the signals decrease and are less distorted when the system is closer to the sliding surface.

The increase of the amplitude of exciting signals to 0.06 m did not indicate the impact of the SMC on the reduction of vertical vibration which is in line with assumptions made during the synthesis

of the SMC. As the time courses of body vertical displacement—with and without SMC—coincide, they are not included in the paper.

Figure 7 presents time courses of the angle φ for the exciting signals frequency of 2 Hz and amplitudes of 0.03 m and 0.06 m. In both cases, limit cycles can be noticed with the system approaching the sliding manifold. In case of the disturbance signal amplitude of 0.03 m (Figure 7a) the maximum value of the signal φ angle with no SMC was 2.31×10^{-3} rad, and 0.21×10^{-3} rad with SMC. The tenfold reduction of the vehicle roll was achieved. In case of 0.06 m amplitude of disturbance signal (Figure 7b)—after reaching the sliding manifold—it can be noticed that signal φ is strongly distorted from the sine wave. The maximum values of angle φ charts for limit cycle with no SMC and with SMC are 4.71×10^{-3} rad, 1.84×10^{-3} rad, respectively. The 2.5-fold reduction of vehicle body roll was achieved in this case. Decreasing of roll reduction efficiency is a result of control signals saturation. This is also the reason why the changes of the angle φ signal is strongly deflected Figure 7b. Figure 8 presents the time courses of the left and right strut control signals for various amplitudes of disturbance. This figure shows (green color) periodic saturation of the left and right strut control signals. Comparison of these signals is additionally shown in Figure 9b.

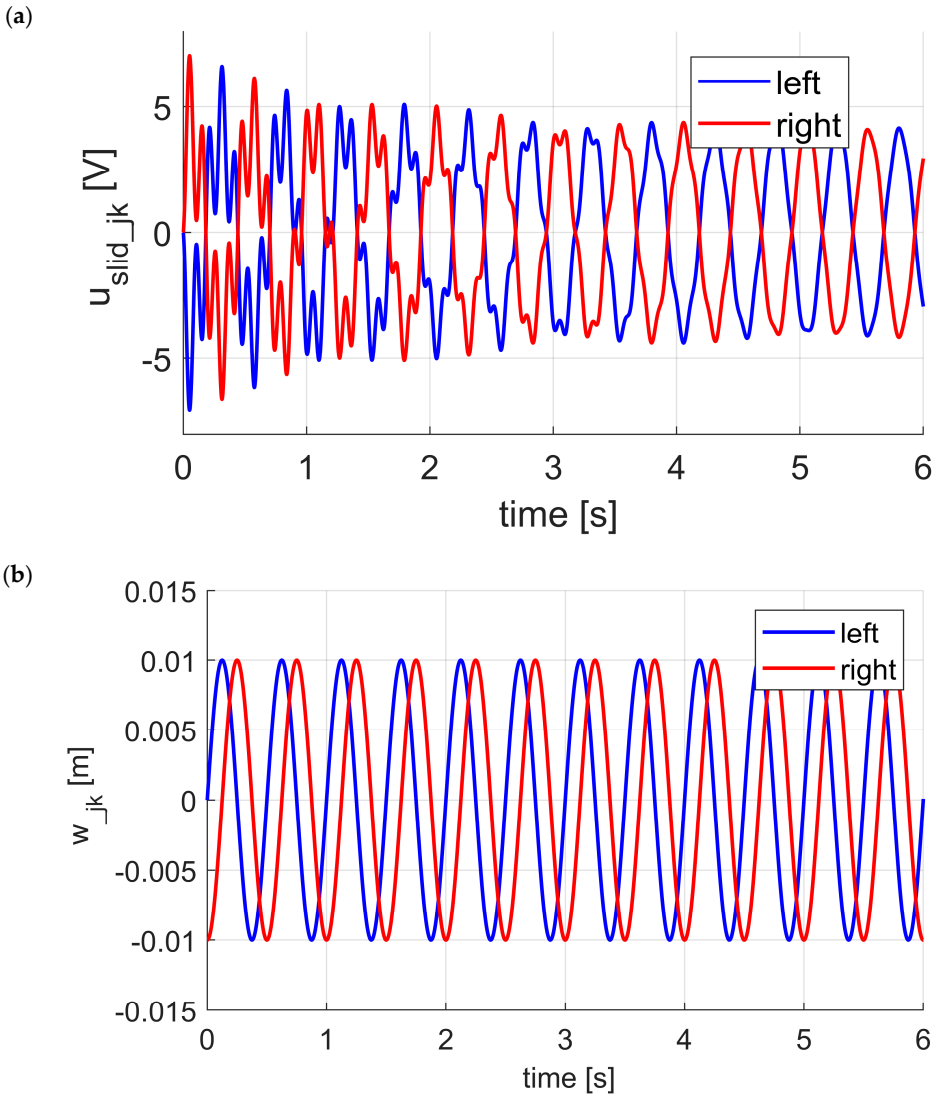

Figure 6. Time courses of the signals generated by the SMC for the left and right strut (**a**) and simulated road disturbances (**b**) for $A_{w\_jR} = A_{w\_jL} = 0.01$ m, $f_{w\_jR} = f_{w\_jL} = 2$ Hz.

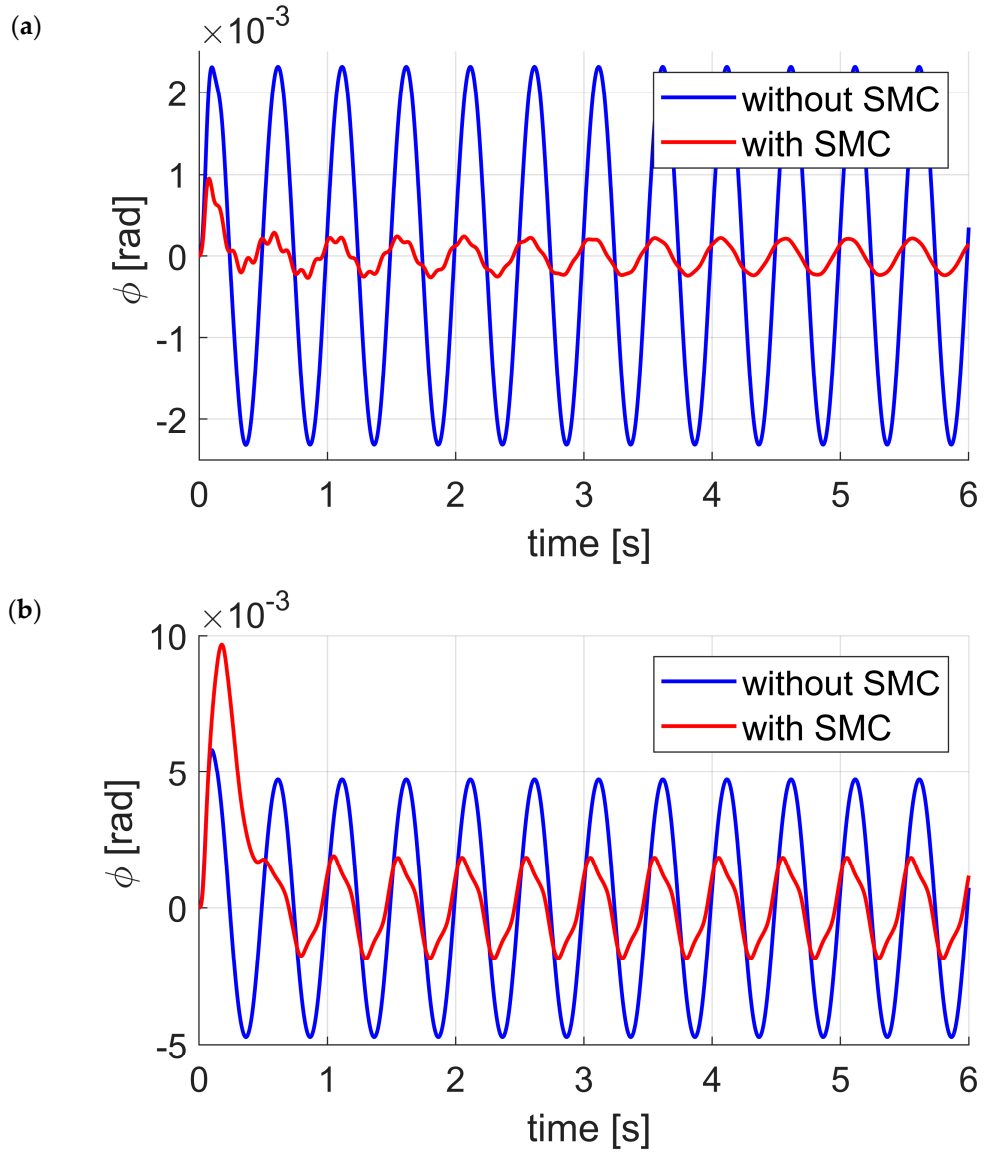

Figure 7. Time courses of variable φ for amplitudes $A_{w\_jR} = A_{w\_jL} = 0.03$ m (**a**), $A_{w\_jR} = A_{w\_jL} = 0.06$ m (**b**).

Figure 9a presents values of the waveform function describing the sliding surface for various amplitudes of disturbance signals. In the case of amplitudes, $A_{w\_jR} = A_{w\_jL} = 0.01$ m, the control system always remains on the sliding surface (blue color), and the strut control signal remains within the permitted range (blue color Figure 8). When the amplitudes of excitations increase up to 0.03 m, the system is taken out from the sliding surface and then, after about 0.1 s, the system trajectories return to the surface. These results from the fact that the right strut control signal becomes saturated at time 0.02 s and 0.2 s (Figure 8b). In case of 0.06 m amplitude, the control system trajectories periodically leave the sliding surface (green color Figures 8 and 9a) because the strut control signal becomes periodically saturated (green color Figures 8 and 9b). In addition to saturation of this signal, one can see the same phase shift as excitation. The struts control signals after reaching a sliding manifold are within the permitted range.

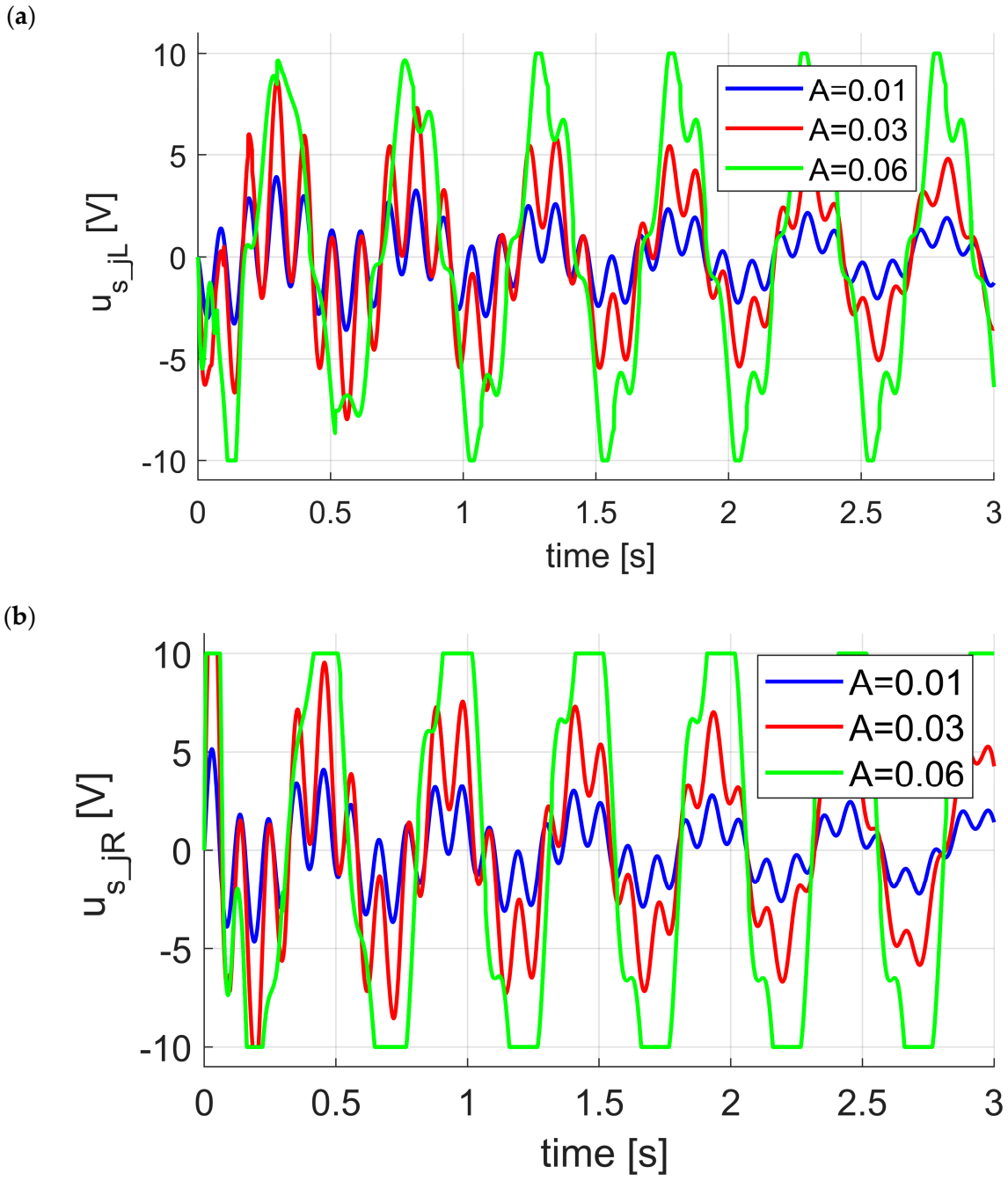

Figure 8. Time courses of the left strut control signal (**a**) and right strut control signal (**b**) for the three different amplitudes of the road disturbances.

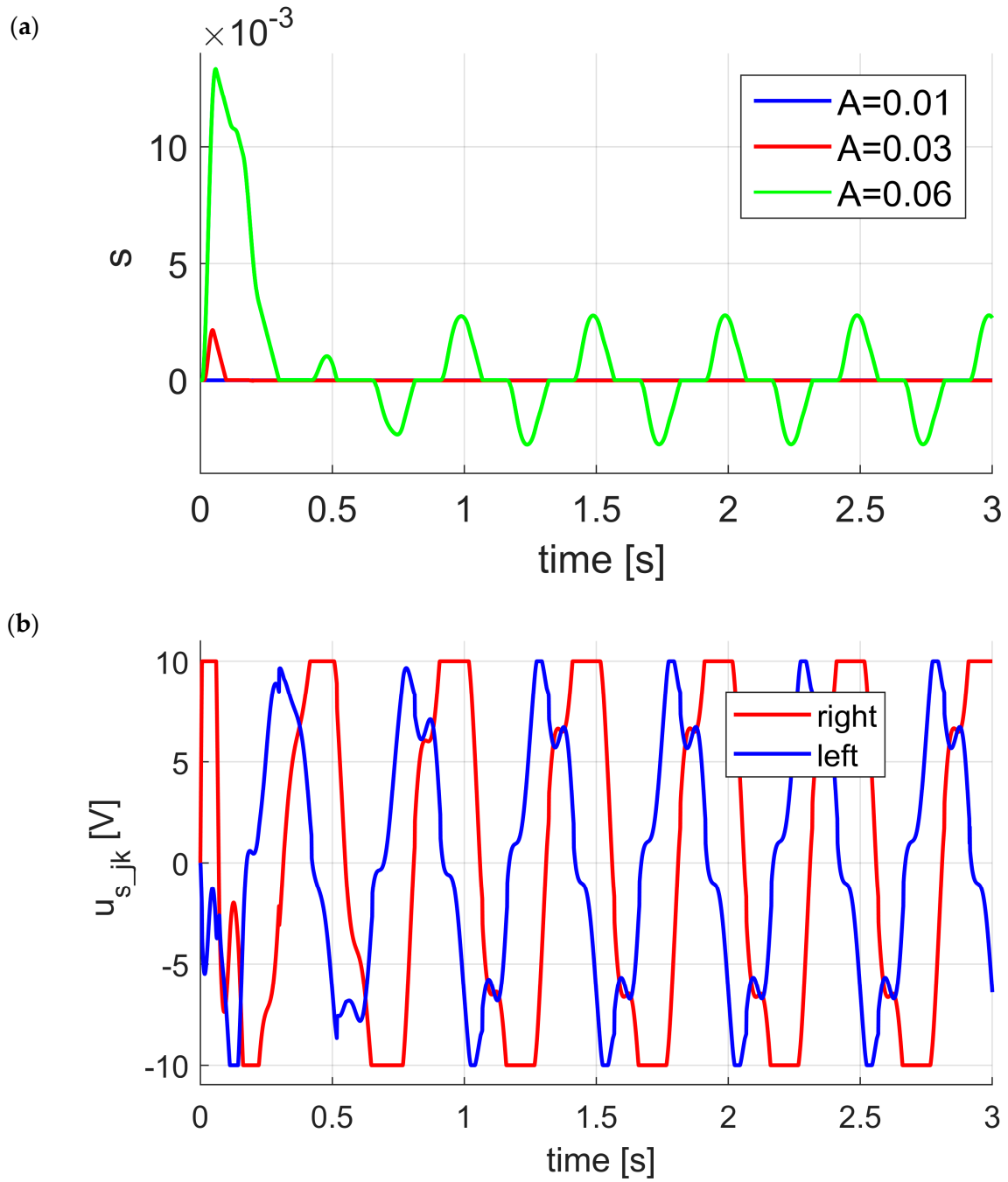

Figure 9. Time courses of the function describing sliding surface for three amplitudes of road disturbances (**a**) and the left and right strut control signals for $A_{w\_jR} = A_{w\_jL} = 0.06$ m, $f_{w\_jR} = f_{w\_jL} = 2$ Hz (**b**).

As one can see the significant advantage of the designed vehicle suspension control system lies in the fact that despite exceeding permitted limits for control signals, the system still reduces the vertical vibration and roll.

One of the most important features of the developed hydraulic actuator is the maximum value of the volumetric flow rate. The flow rate in servovalve was calculated based on Equation (113).

$$Q_{s\_jk} = u_{r\_jk} l C_d \sqrt{\frac{P_z - P_{r\_jk} \cdot sign\left(u_{r\_jk}\right)}{\rho}} \tag{113}$$

To evaluation of designed controller P_{ins_jk}, P_{max_jk}, E_{mod}, P_{lc_max} energetic indicators were used. The instantaneous power P_{ins_jk} generated by the actuator is presented by the Formula (114).

$$P_{ins\_jk} = Q_{s\_jk} \cdot P_{r\_jk} \tag{114}$$

One of the basic indicators used in the selection of the actuators is the power demand P_{max_jk} (115). This indicator allows the selection of the hydraulic power supply unit. The control system of the hydraulic actuators must work without overstepping the specified maximum power [32].

$$P_{max\_jk} = \max\left(P_{ins\_jk}\right) \tag{115}$$

Indicator E_{mod} (116) and (117) estimates the energy demand of the vibration reduction system. In this indicator, the modulus of instantaneous power is averaged. This definition implies that there is no energy harvesting from the suspension system [32,33]. Modulus of instantaneous power in Equations (116) and (117) is a result of applying servovalve. Strut actuator moves up and down thanks to servovalve action. Independently of move direction the power is taken from a hydraulic power supply and is always positive. The product of the averaged instantaneous modulus of power P_{mod} and unit of time (one second) is an energy E_{mod}. This energy is used by the system during one second.

$$P_{mod} = \frac{1}{T_o} \int_0^{T_o} \left| P_{ins\_jk} \right| dt \tag{116}$$

$$E_{mod} = P_{mod} \times 1 \cdot s \tag{117}$$

where T_o—is observation time.

The maximum value of the instantaneous power when the state trajectory is approaching the limited cycle is denoted P_{lc_max}. This indicator is of great importance for the evaluation of hydraulic actuator energy demand and designing the hydraulic power supplier.

Comparison of the flow rates in servovalves controlling both struts actuators for excitation parameters was presented in Figure 10a. The maximum value of flow rate for left strut ($Q_{s\_jL} = 4.269 \cdot 10^{-4} \frac{m^3}{s}$) is less than for right strut ($Q_{s\_jR} = 5.521 \cdot 10^{-4} \frac{m^3}{s}$). It is due to the assumed initial conditions, developed model of disturbances (Figure 6b) and the transient states which are the result of them. Values of the flow rates for left and right strut are similar when the state trajectory is approaching the limited cycle and are equals $Q_{s\_jL} = 1.946 \cdot 10^{-4} \frac{m^3}{s}$, $Q_{s\_jR} = 2.785 \cdot 10^{-4} \frac{m^3}{s}$, respectively. Comparison of the left strut actuator flow rates in servovalve for different excitation amplitudes is presented in Figure 10b. As one can see the higher amplitude of excitation involved the significant increase of the flow rates. Values Q_{s_jk} are important during the design of the hydraulic system and especially on the stage of servovalve selection. The maximum values of flow rates for excitations amplitudes 0.001, 0.003 and 0.006 are equals $Q_{s\_jL} = 1.963 \cdot 10^{-4} \frac{m^3}{s}$, $Q_{s\_jL} = 4.269 \cdot 10^{-4} \frac{m^3}{s}$, $Q_{s\_jL} = 4.905 \cdot 10^{-4} \frac{m^3}{s}$, respectively.

In Figure 11a comparison of instantaneous power used by left strut actuator with and without SMC are presented. The time courses of the instantaneous power without SMC show that their values are similar for whole chart. Maximum values equal $P_{max\_jL} = 35.68$ W and $P_{lc\_max} = 35.45$ W. However, for system with SMC values of instantaneous power was significantly higher at the beginning of the chart $P_{max\_jL} = 109.4$ W. After reaching limited cycle system with SMC need 10 W less power than system without SMC. It is due to the fact that the addition of the SMC responsible for roll control involves the optimal work of the LQR. These controllers were synthesized for the assumption of independent operation of struts.

Values of proposed indicators for all excitation amplitudes were summarized in Table 1.

Table 1. Comparison of power consumption indicators for the system with SMC and with No SMC.

Control Type	Amplitude	P_{max_jL} (W)	P_{lc_max} (W)	E_{mod} (J)
No SMC	$A = 0.01$	35.68	35.45	16.63
SMC		109.4	25.49	12.78
No SMC	$A = 0.03$	322.8	321.0	150.6
SMC		546.55	253.6	99.61
No SMC	$A = 0.06$	1290.8	1286.4	609.3
SMC		1709.5	839.22	418.21

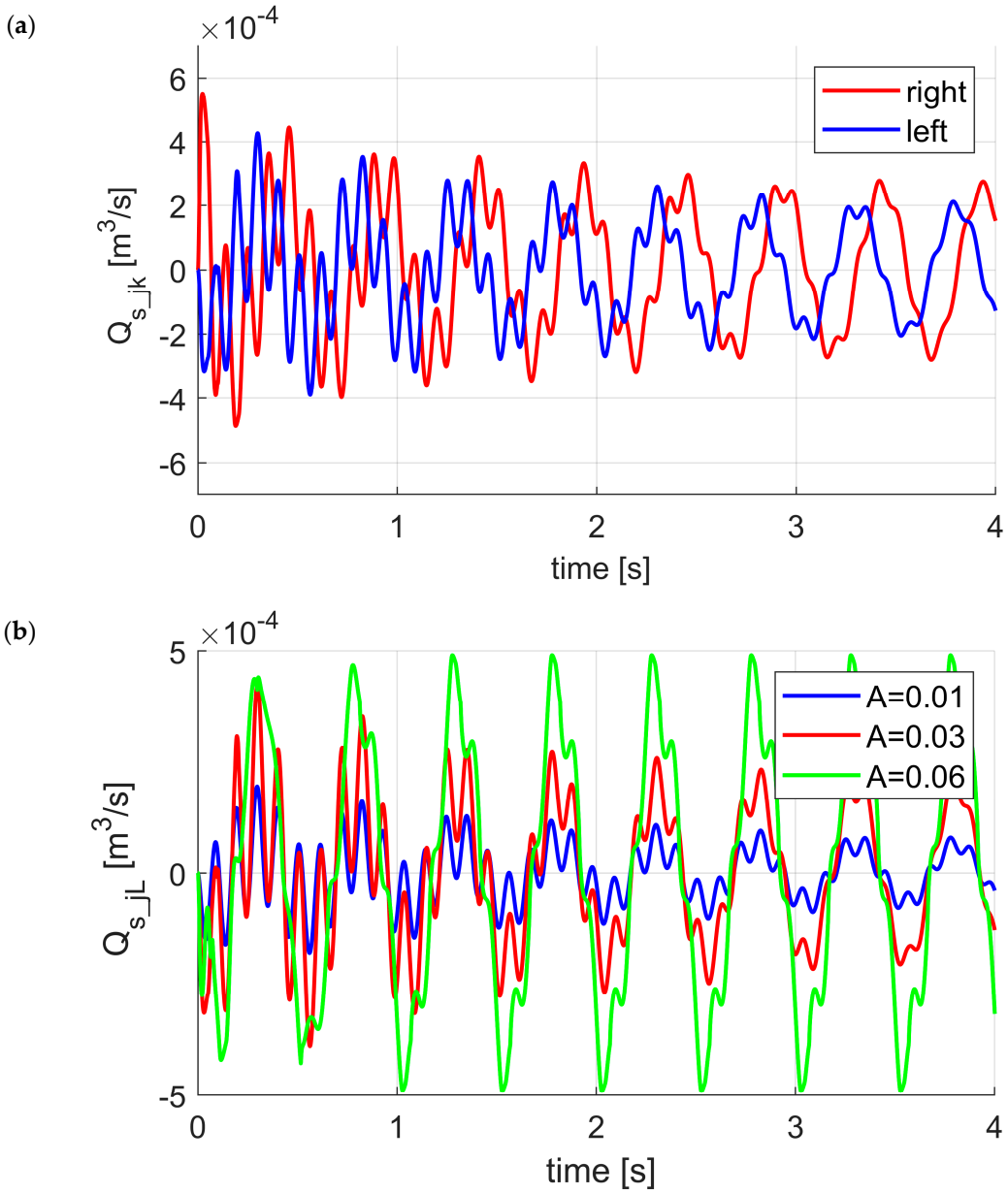

Figure 10. Comparison of the flow rates in servovalves of left and right strut actuators for excitation parameters $A_{w\_jR} = A_{w\_jL} = 0.03$ m, $f_{w\_jR} = f_{w\_jL} = 2$ Hz (**a**) and comparison of the left strut actuator flow rates in servovalve for different excitation amplitudes (**b**).

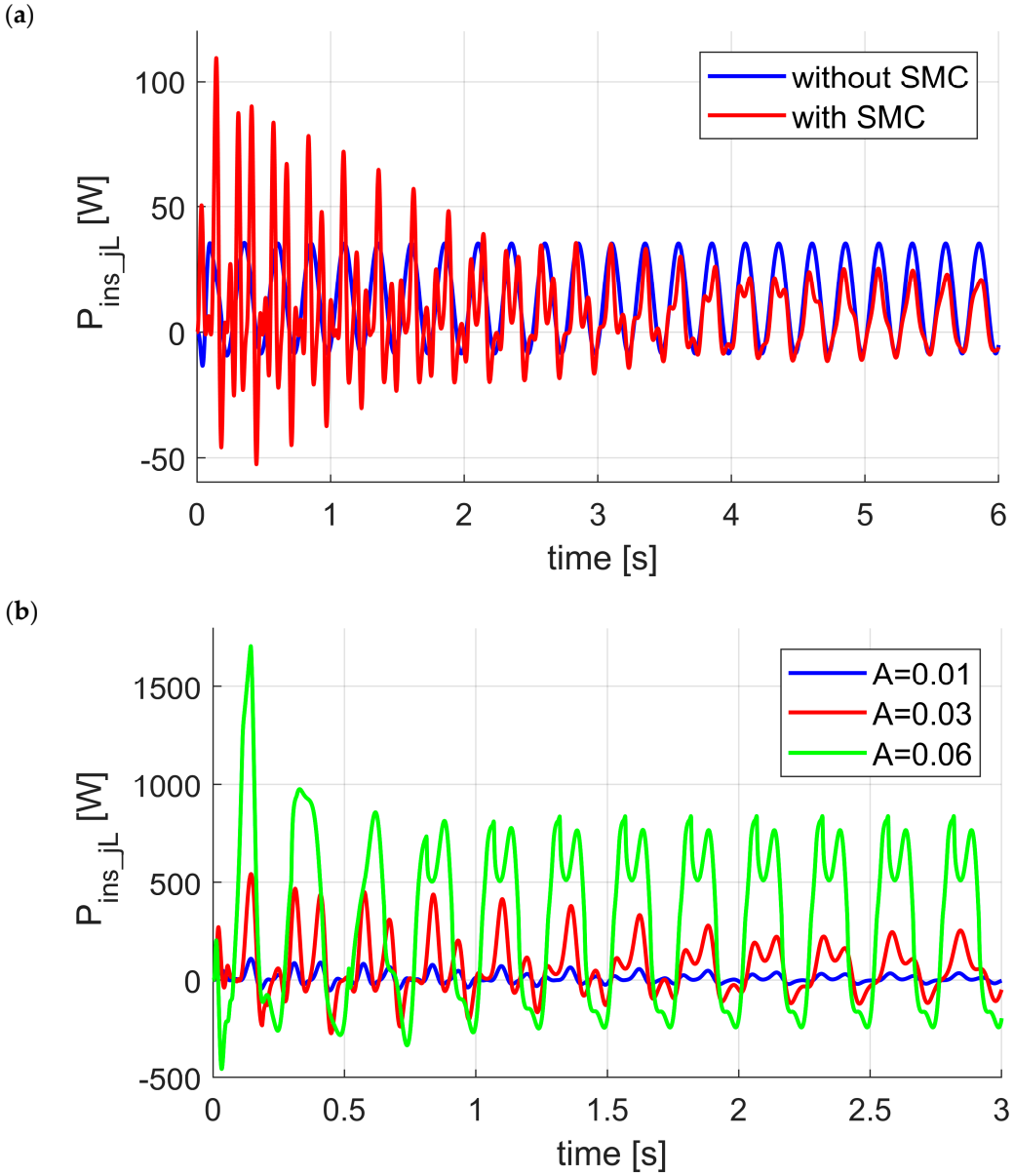

Figure 11. Comparison of strut actuator power consumptions with and without SMC controller for excitation parameters $A_{w\_jR} = A_{w\_jL} = 0.01$ m, $f_{w\_jR} = f_{w\_jL} = 2$ Hz (**a**) and comparison of the left strut actuator power consumption for different excitation amplitudes (**b**).

Analyzing of data presented in Table 1 especially values of E_{mod} one can see that using the system with SMC gave significant advantages in energy consumptions. The highest energy demand was observed for the largest tested amplitude of excitation. For each considered case the energy demand was lower for the system with SMC. A similar result can be seen for consideration of the highest instantaneous power when the state trajectory is approaching the limited cycle P_{lc_max}. However, the opposite result can be observed for maximum instantaneous power P_{max_jk}. If the system trajectory is remaining on the sliding surface, the SMC controller generates equivalent signals $u_{slid\_jR} = -0.5u^{-}_{eq\_slid\_j}$, $u_{slid\_jL} = 0.5u^{-}_{eq\_slid\_j}$ that synchronize the displacements z_{s_jL} and z_{s_jR} (the actuator fixing points to the body car) in the presence of disturbances from the road irregularities. This means that angle φ does not change. Moreover, the signals u_{slid_jR}, u_{slid_jL} differ only in the sign. The energy of these control signals do not increase therefore, the energy demand of the active suspension system does not increase too. In the case when the system trajectory is out of the sliding surface,

there is an additional component of the signals generated by the SMC $Msign(s(x^{-}))$. This implies an increase of the control signal energy and thus an increase of the energy demand of the entire system. For this reason, in the initial time, the energy demand is higher than the system reaches the sliding surface. This phenomenon can be seen in Figure 11.

6. Conclusions

Presented in the paper results of the research clearly have shown that the proposed ASMC controller is effective in roll and vibration reduction. The research presented in this work was carried out with the use of SIL simulation method. These tests show the correctness of the ASMC synthesis method which is based on controllers for the individual struts and anti-roll functionality.

The main advantage of the proposed system is the roll reduction without increasing the energy demand for active vehicle suspension. It was achieved thanks to the proposed ASMC control structure. The system directly controls vehicle suspension struts by using LQR method, which ensures the reduction of vertical vibration while the role of the SMC controller is to reduce the rolling of the vehicle.

The vehicle suspension model was decomposed into two subsystems. Synthesis of SMC controller was developed for the subsystem responsible for the roll of the vehicle. Whereas controllers LQR were designed to vertical vibration reduction.

The proposed method simplifies the selection of SMC parameters because instead of analyzing one complicated control synthesis problem, two independent tasks of the two times lower order are considered.

Disturbances existing in wheeled vehicle suspensions could cause significant deterioration of quality factors used to control law evaluation. In case of SMC they could cause of unreachability of sliding surface. SMC controller synthesis proposed in the paper guarantees convergence of closed loop system trajectory to the selected sliding surface in the presence of disturbance signals. Conducted numerical tests verified mathematical thesis proved in the paper. During simulation tests it was observed that the system was taken out of the sliding surface in case of demanded control signals were out of permitted range. The presented method can be applied to other systems [13] disturbed by harmonic excitation.

The vehicle roll depends on various factors which are hard to predict. It was the reason for choosing an SMC which belongs to the robust category. The performed tests have shown that the designed SMC alleviates the vehicle roll however, does not affect the reduction of vertical displacements. Vertical vibration reduction is ensured by LQR controllers related directly to suspension struts. The conducted tests show that power demand, for achieving the desired vibration reduction, decreases within reaching the selected sliding surface. A similar phenomenon is observed during analysis of volumetric flow rates. Due to the proposed ASMC structure, the controller responsible for roll reduction did not enlarge energy consumption. It is since roll reduction involves the optimal work of the LQR. These controllers were synthesized for the assumption of independency of struts operation. The concept of future work assumes research with usage of full vehicle suspension model, taking into account other phenomena e.g., pitch and yaw.

Author Contributions: Conceptualization, J.K., M.S. and W.R.; methodology, J.K., M.S. and W.R.; software, M.S.; validation, J.K., M.S. and W.R.; formal analysis, M.S.; investigation, J.K., M.S. and W.R.; writing—original draft preparation, W.R.; writing—review and editing, J.K.; funding acquisition, J.K. All authors have read and agreed to the published version of the manuscript.

Funding: This work was supported by National Centre for Research and Development of Poland (research project No. PBS3/B6/27/2015).

Conflicts of Interest: The authors declare no conflict of interest.

References

1. Colombo, E.F.; Di Gialleonardo, E.; Facchinetti, A.; Bruni, S. Active carbody roll control in railway vehicles using hydraulic actuation. *Control Eng. Pract.* **2014**, *31*, 24–34. [CrossRef]
2. Cronjé, P.H.; Els, P.S. Improving off-road vehicle handling using an active anti-roll bar. *J. Terramech.* **2010**, *47*, 179–189. [CrossRef]
3. Vu, V.T.; Sename, O.; Dugard, L.; Gaspar, P. Active anti-roll bar control using electronic servo valve hydraulic damper on single unit heavy vehicle. *IFAC-PapersOnLine* **2016**, *49*, 418–425. [CrossRef]
4. Vu, V.T.; Sename, O.; Dugard, L.; Gaspar, P. H-inv active anti-roll bar control to prevent rollover of heavy vehicles: A robustness analysis. *IFAC-PapersOnLine* **2016**, *49*, 99–104. [CrossRef]
5. Her, H.; Yi, K.; Suh, J.; Kim, C. *Development of Integrated Control of Electronic Stability Control, Continuous Damping Control and Active Anti-Roll Bar for Vehicle Yaw Stability*; IFAC: Berlin, Germany, 2013; Volume 7, ISBN 9783902823434.
6. Vu, V.T.; Sename, O.; Dugard, L.; Gaspar, P. Enhancing roll stability of heavy vehicle by LQR active anti-roll bar control using electronic servo-valve hydraulic actuators. *Veh. Syst. Dyn.* **2017**, *55*, 1405–1429. [CrossRef]
7. Bayrakceken, H.; Tasgetiren, S.; Aslantas, K. Fracture of an automobile anti-roll bar. *Eng. Fail. Anal.* **2006**, *13*, 732–738. [CrossRef]
8. Muniandy, V.; Samin, P.M.; Jamaluddin, H. Application of a self-tuning fuzzy PI-PD controller in an active anti-roll bar system for a passenger car. *Veh. Syst. Dyn.* **2015**, *53*, 1641–1666. [CrossRef]
9. Schumann, A.R.; Anderson, R.J. Optimal control of an active anti roll suspension for an off-road utility vehicle using interconnected hydragas suspension units. *Veh. Syst. Dyn.* **2002**, *37*, 145–156. [CrossRef]
10. Chu, D.; Lu, X.Y.; Wu, C.; Hu, Z.; Zhong, M. Smooth Sliding Mode Control for Vehicle Rollover Prevention Using Active Antiroll Suspension. *Math. Probl. Eng.* **2015**, *2015*. [CrossRef]
11. Kunnappillil Madhusudhanan, A.; Corno, M.; Holweg, E. Sliding mode-based lateral vehicle dynamics control using tyre force measurements. *Veh. Syst. Dyn.* **2015**, *53*, 1599–1619. [CrossRef]
12. Muniandy, V.; Mohd Samin, P.; Jamaluddin, H.; Abdul Rahman, R.; Abu Bakar, S.A. Double anti-roll bar hardware-in-loop experiment for active anti-roll control system. *J. Vibroeng.* **2017**, *19*, 2886–2909. [CrossRef]
13. Konieczny, J.; Sibielak, M.; Raczka, W. The Control System for a Vibration Exciter. *Solid State Phenom.* **2013**, *198*, 600–605. [CrossRef]
14. Konieczny, J.; Sibielak, M.; Rączka, W. Sliding mode controller for vehicle body roll reduction using active suspension system. In *Structural Health Monitoring, Photogrammetry & DIC*; Conference Proceedings of the Society for Experimental Mechanics Series; Springer: New York, NY, USA, 2019; Volume 6, pp. 199–203.
15. Savaresi, S.M.; Poussot-Vassal, C.; Spelta, C.; Sename, O.; Dugard, L. *Semi-Active Suspension Control Design for Vehicles*; Elsevier: Amsterdam, The Netherlands, 2010; ISBN 9780080966786.
16. Hrovatt, D. Optimal Active Suspension Structures for Quarter-car Vehicle Models. *Automatica* **1990**, *26*, 845–860. [CrossRef]
17. Yue, C.; Butsuen, T.; Hedrick, J.K. Alternative Control Laws for Automotive Active Suspensions. *J. Dyn. Syst. Meas. Control* **1989**, *111*, 2373–2378. [CrossRef]
18. Wrona, S.; Pawelczyk, M. Shaping frequency response of a vibrating plate for passive and active control applications by simultaneous optimization of arrangement of additional masses and ribs. Part I: Modeling. *Mech. Syst. Signal Process.* **2016**, *70*, 682–698. [CrossRef]
19. Wrona, S.; Pawelczyk, M. Shaping frequency response of a vibrating plate for passive and active control applications by simultaneous optimization of arrangement of additional masses and ribs. Part II: Optimization. *Mech. Syst. Signal Process.* **2016**, *70–71*, 699–713. [CrossRef]
20. Czop, P.; Mendrok, K.; Uhl, T. Application of inverse linear parametric models in the identification of rail track irregularities. *Arch. Appl. Mech.* **2011**, *81*, 1541–1554. [CrossRef]
21. Maciejewski, I.; Kiczkowiak, T.; Krzyzynski, T. Application of the Pareto-optimal approach for selecting dynamic characteristics of seat suspension systems. *Veh. Syst. Dyn.* **2011**, *49*, 1929–1950. [CrossRef]
22. Kciuk, S.; Duda, S.; Mężyk, A.; Świtoński, E.; Klarecki, K. Tuning the Dynamic Characteristics of Tracked Vehicles Suspension Using Controllable Fluid Dampers. In *Innovative Control Systems for Tracked Vehicle Platforms*; Springer: Cham, Switzerland, 2014; pp. 243–258.
23. Azar, A.T.; Zhu, Q. Advances and applications in sliding mode control systems. *Stud. Comput. Intell.* **2015**, *576*, 1–42. [CrossRef]

24. Sibielak, M.; Konieczny, J.; Kowal, J.; Rączka, W.; Marszalik, D. Optimal Control of Slow-Active Vehicle Suspension—Results of Experimental Data. *J. Low Freq. Noise Vib. Act. Control* **2013**, *32*, 99–116. [CrossRef]
25. Sibielak, M.; Raczka, W.; Konieczny, J.; Kowal, J. Optimal control based on a modified quadratic performance index for systems disturbed by sinusoidal signals. *Mech. Syst. Signal Process.* **2015**, *64–65*, 498–519. [CrossRef]
26. Sibielak, M.; Raczka, W.; Konieczny, J. Modelling and control of a full vehicle active suspension system. In Proceedings of the 2019 20th International Carpathian Control Conference, ICCC 2019, Krakow-Wieliczka, Poland, 26–29 May 2019.
27. Lozia, Z.; Zdanowicz, P. Optimization of damping in the passive automotive suspension system with using two quarter-car models. In Proceedings of the Scientific Conference on Automotive Vehicles and Combustion Engines (KONMOT 2016), Krakow, Poland, 22–23 September 2016; Volume 148, p. 012014. [CrossRef]
28. Lozia, Z. A two-dimensional model of the interaction between a pneumatic tire and an even and uneven road surface. *Veh. Syst. Dyn.* **1988**, *17*, 227–238. [CrossRef]
29. Konieczny, J.; Kowal, J.; Rączka, W.; Sibielak, M. Bench Tests of Slow and Full Active Suspensions in Terms of Energy Consumption. *J. Low Freq. Noise Vib. Act. Control* **2013**, *32*, 81–98. [CrossRef]
30. Viersma, T.J. Analysis, synthesis and design of hydraulic servosystems and pipelines. *J. Dyn. Sys. Meas. Control* **1980**, *103*, 73. [CrossRef]
31. Hedrick, J.K.; Donahue, M.D. Implementation of an Active Suspension. Preview Controller for Improved Ride Comfort. In *Nonlinear and Hybrid Systems in Automotive Control*; Springer: London, UK, 2003; pp. 1–22. ISBN 978-1-85233-652-3.
32. Konieczny, J.; Rączka, W.; Sibielak, M.; Kowal, J. Energy Consumption of an Active Vehicle Suspension with an Optimal Controller in the Presence of Sinusoidal Excitations. *Shock Vib.* **2020**, *2020*, 6414352. [CrossRef]
33. Kowal, J.; Pluta, J.; Konieczny, J.; Kot, A. Energy Recovering in Active Vibration Isolation System—Results of Experimental Research. *J. Vib. Control* **2008**, *14*, 1075–1088. [CrossRef]